CHERENKOV DETECTION OF GAMMA RAYS AND COSMIC HADRONS

Cherenkov Array at Thémis

C A T

Project report

Project for a development on the site of the

systems THÉMISTOCLE & ASGAT at Thémis associating wave-front sampling with high-definition imaging

---

CHERENKOV DETECTION OF GAMMA RAYS AND COSMIC HADRONS

Cherenkov Array at Thémis

C A T

Project report

Project for a development on the site of the systems THÉMISTOCLE & ASGAT at Thémis associating wave-front sampling with high-definition imaging

France :

Bernard Degrange [b], Robert Bazer-Bachi [d], Jean-Noël Capdevielle [i], Bernard Fabre [g], Patrick Fleury [b], Gérard Fontaine [b], Roger George[c], Claude Ghesquière [a], Philippe Goret [e], Christian Gouiffes [e], Isabelle Grenier [e,f], Christian Meynadier [g], Ung Nguyen-Khac [b], Eric Paré [b], Yvette Pons [c], Michael Punch [b], Monique Rivoal [c], Bruno Rivoire [h], Marcel Urban [b] & Jirka Vrana [b].

Other countries :

Paul Baillon (CERN) [j], David Fegan (Ir.) [k]
Thomas Palfrey (USA) [l]
Gianni Navarra & Carlo Morello (It.) [m]

[a] LPC - Collège de France & IN2P3;
[b] LPNHE- Ecole Polytechnique & IN2P3;
[c] LPNHE- Universités Paris 6-7 & IN2P3;
[d] CESR, Toulouse & INSU;
[e] SAp - DAPNIA, CEA-Saclay;
[f] Université Paris 7;
[g] Université de Perpignan;
[h] IMP Odeillo-Perpignan, CNRS;
[i] LPT-Université de Bordeaux1;
[j] CERN;
[k] University College, Dublin, Ireland;
[l] Purdue University, Indiana, USA;
[m] CNR-INFN, Torino, Italy.

CAT
Project Report

Table of Contents

I. The development of the Thémis site for the detection of cosmic-ray showers

I.1 Recent developments in γ-ray astronomy

The last decade has been marked by theoretical and experimental progress which has deeply modified the goals of γ-ray astronomy.

I.1.1 On the theoretical side

On the theoretical side, the application to cosmology of ideas coming from particle physics has led to important predictions to verify: for example, "Super-symmetry" implies the existence of new stable particles: the "Neutralinos". Their mass must be greater than 50 GeV (otherwise they would have been observed in current collider experiments) but cannot be too much above the mass scale of weak bosons and must not be greatly above a TeV (Ref. 1). Such stable particles, produced in the first moments of the Universe and subsequently decoupled, could today constitute all or part of the dark matter if that is non-baryonic in nature (Ref. 2). The domain of mass anticipated is found to be precisely that which leads to a Euclidean universe (Ω=1) predicted by "inflationary" scenarios. Such particles can today, by mutual annihilation, produce high-energy particles, γ's in particular. In general, traces of the original universe are sources of cosmic rays (Ref. 3) just as much as accelerating systems such as shock waves produced in various astrophysical objects (Supernovæ, Pulsars, Active Galactic Nuclei). This gives a renewed interest in cosmic rays, of which γ's are the most interesting since, as they propagate in straight lines, they often allow identification of their source with a known object (by observation in Radio, IR, Visible, UV...).

I.1.2 SATELLITE AND GROUND-BASED OBSERVATION

With regard to observations, the COS-B satellite and more recently GRO (Gamma-Ray Observatory) have discovered several intense sites of acceleration, sources of high-energy γ's; the first four of these are pulsars in our own galaxy (the Crab, Vela, Geminga and PSR 1706-44), but more importantly another score are much more distant objects (and thus very intense emitters of γ's): Active Galactic Nuclei (AGN). Aboard the GRO satellite, the EGRET detector measures the energy spectrum up to 30 GeV; above this the flux is too weak for the available detecting surface. So, we are obliged to resort to ground-based devices which detect γ's indirectly, through the intermediary of the large electromagnetic showers that they produce in the atmosphere. This technique has long remained unreliable because of the enormous background noise of the flux of charged cosmic rays which the first-generation instruments could not separate from the γ-signal.

I.1.3 PROSPECTS FOR OBSERVATIONS USING CHERENKOV LIGHT

Ground-based γ astronomy was truly born in 1989-90 with the evolution of techniques which allowed the efficient identification of atmospheric electromagnetic showers. All these apparatuses detect Cherenkov radiation emitted in the atmosphere by relativistic particles. To reduce the isotropic background noise of charged cosmic rays, the angular resolution has been improved to the order of a milliradian. The other discriminating factor found to be critical is the angular structure of the shower, analysed in the "Cherenkov imaging" technique. This consists of placing in the focal plane of a large mirror a camera containing an array of photo-multipliers (PM's). Another recently developed technique consists of using a large field of mirrors to allow very precise time-sampling of the Cherenkov wave-front whose reconstruction gives the direction of the shower with good angular resolution.

The first significant result came from the Whipple Observatory on Mount Hopkins (USA) which, using the imaging technique, discovered in 1989 the continuous signal from the Crab nebula (Ref. 4) in the TeV range. This observation was confirmed soon thereafter (1990) by the French groups ASGAT (above 600 GeV) (Ref. 5) and THÉMISTOCLE (above 3 TeV) (Ref. 6) using the sampling technique, and very recently by the German-Spanish experiment HEGRA in the Canaries using an imaging detector (Ref. 7). Lastly, another pulsar (PSR 1706-44) has just been observed from the southern hemisphere by the Australian-Japanese group CANGAROO with an imaging device (Ref. 8).

In the meantime, in 1992, an active galactic nucleus was observed by the Whipple Observatory group (Ref. 9) in the TeV region: it is a BL-Lacertæ type object, "Markarian 421", which was already in the catalogue of sources observed by the EGRET detector aboard the GRO satellite. It is significant that the most intense extra-galactic source in this catalogue, the quasar 3C279, has not been observed; it is a very distant object (with a spectral red-shift of $z = 0.54$), whereas "Markarian 421" is the "nearest" source to earth in the catalogue ($z = 0.03$). These observations can be interpreted by the absorption of TeV γ's which interact with the diffuse intergalactic infra-red radiation according to: $\gamma + \mathrm{IR\ photon} \rightarrow e^{+} + e^{-}$. By extrapolating the energy spectra of sources as distant as 3C279 as measured by EGRET and taking into account this absorption, such objects are predicted to be accessible with atmospheric Cherenkov telescopes if the threshold energy is lowered to about 100 GeV (Ref. 10). Observations of distant quasars at such energies would confirm the above explanation and provide the first measurement of the extra-galactic infra-red light.

With three currently active sources (one extra-galactic), ground-based γ-astronomy has entered its maturity. The next step is evidently to build detectors with lower threshold energies so as to cover the unexplored region of the spectrum between 30 and 400 GeV. The stakes are high: the cut-off energy in a spectrum can reflect either the maximum accelerating energy of charged particles, or an absorptive phenomenon for a distant source; in particular, it is in this range that the possible annihilation of neutrinos could be discovered, for example, in the form of a ray if the annihilation produces only two photons (Ref. 11).

I.1.4 AT NATIONAL LEVEL

In France, experimental work on high-energy cosmic rays — considerably reduced in the past 20 years — has started again at the end of the 80's with the ASGAT, THÉMISTOCLE, and ARTÉMIS groups. The first two experiments used the technique, then new, of wave-front sampling, each in a different energy domain, using the site of the old solar power-station THÉMIS (eastern Pyrenees) after it was abandoned by Electricité de France. The ASGAT experiment of SAp Saclay aimed at low energies (600 GeV threshold) with seven large mirrors of 38 m² each. The THÉMISTOCLE experiment including several laboratories of IN2P3 had been approved in a reduced version to validate the sampling technique; in this context the device consists of only eighteen 0.5 m² mirrors, giving a 3 TeV threshold. After one year of operation, both experiments were able to observe a significant signal from the Crab Nebula in their respective domains and THÉMISTOCLE has shown that the spectrum extended continuously up to 15 TeV. Moreover, the ARTÉMIS group, using the 10 m diameter Whipple Observatory telescope where they experimented with a UV camera, were able to familiarise themselves with the imaging technique and demonstrate the signal from the Crab Nebula in the UV. The conditions are now assembled to place on the THÉMIS site a set of instruments including, besides the current ASGAT and THÉMISTOCLE installations, an imaging telescope whose threshold would be about 200 GeV. This project, named CAT (Cherenkov Array at THÉMIS), will allow at the one time the accomplishment of original observations at currently inaccessible energies and the exploration of other techniques: very-high-resolution imaging and the associated "image-sampling", with a view to preparing a large international project. Its still distant aim of a 20 to 30 GeV threshold will not in fact be reached in a single step.

I.2 Cherenkov methods: sampling, imaging and others...

I.2.1 A Few Numbers

Cosmic showers emit Cherenkov photons principally in directions close to the axis of propagation of the initiating cosmic particle, illuminating the ground in a nearly uniform manner around the impact point of the shower up to distances of about 120 m, thus over a surface of

$$S \approx 5 \times 10^4 \text{ m}^2.$$

The number of detected photons, or photo-electrons (γe), taking into account the transparency of the atmosphere and collection efficiencies of the mirrors and photo-multipliers, is (in the TeV range) about

$$20 \text{ γe / TeV / m}^2.$$

This light is received in the form of a flash, so that the sky noise interferes only in inverse proportion to the detector speed. The level of sky noise is well known, and its observations from many different sites agree. Specifically, this noise integrated over an angle of acceptance of ±25 mrad (typical of the useful acceptance for the study of a point cosmic source) expressed in γe is of order:

$$0.3 \text{ γe / ns / m}^2.$$

The major part of this noise is stochastic in time and direction. However, the difficulties are amplified by certain non-stochastic contributions. The illumination of bright stars which may be in the neighbourhood of the source under study must be taken into account, as must the high-energy Cherenkov radiation from energetic muons close to a mirror, and also direct collisions of secondary cosmic particles on the camera.

The most severe noise is still that due to showers induced by charged cosmic hadrons. Towards 1 TeV, the rate of hadronic showers for an angle of acceptance of ±25 mrad is 1000 times higher than that of γ's from the Crab. The instrumental strategy will have to emphasise the differentiation between a γ-shower and a hadron shower.

I.2.2 Different instrumental methods

To satisfy the requirements of large collection over a short time-scale, all detectors use mirror optics and photo-multiplier detectors. From these two elements, strategies vary as to whether one takes more or less advantage of time or of arrival direction of the photons.

I.2.2.1 Time Sampling

The two devices currently available on the THÉMIS site concentrate on time measurements to determine the shape of the wave-front, using a sampler divided into 7 mirrors for ASGAT and 18 for THÉMISTOCLE. However, on ASGAT, subdivision of the field of the camera to take account of the size of the images is being developed using separate readings from 7 PM's in each camera. In a similar way for THÉMISTOCLE, tests are planned — in association with the Italian group

EAS-Top — for subdivision of the focal plane with the aid of a 64-pixel multi-anode PM. The CAT project will be the occasion to test in other forms the potentialities for the association of the sampling and imaging techniques.

I.2.2.2 Imaging, towards high resolution

The imaging method has been chiefly worked out by the Whipple team on the basis of a unique telescope containing 75 m^2 of mirrors and with an optical precision of the order of a mrad. The shower image is read with a pixel resolution of diameter $\varnothing \approx 4.1$ mrad. Parallel to technical progress, the imaging method has been refined by studies of simulations of γ- and hadron showers (mainly by Michael Hillas). The CAT project involves as its main component the design of an imaging device whose conception borrows much from the work of the Whipple group. Principally, the evolution towards a finer imaging device, started in 1988 by the change from 37 to the current 109 PM camera, has greatly improved performance, verifying models for atmospheric showers and encouraging further again this line of development. The recent results of the Japanese CANGAROO project have just brought encouragement in this regard, since with a much smaller mirror but finer imaging they could discover in a few hours of observation a cosmic source of comparable intensity to the Crab.

I.2.2.3 Stereo Imaging

Imaging associating several telescopes on a site has been used, in particular by Turver at Narrabri and by Stepanian in the Ukraine, allowing "stereo" observation of showers. A field of a score of telescopes of the same kind as Whipple's has also been suggested: the CASITA project. The GRANITE project, currently being tested at the Whipple Observatory site, associates with the existing telescope a second one of similar size, and shows what CASITA could achieve. The imaging project of the HEGRA group at the Las Palmas site foresees the installation of 5 smaller imaging devices.

I.2.2.4 Method with a large number of mirrors

A completely different strategy has been envisaged which uses a vast ensemble of mirrors to reach thresholds of about 10 GeV and perhaps to join up to the energy range of satellite observations. In the past few years, calculations have been done by Tümer with a view to reusing the solar power-station Solar-1 in California. We have repeated these estimates with elements of the THÉMIS oven. Although there does not appear to be an obstacle in principle, preliminary studies are imperative, and tests on accelerators will be useful principally to validate the simulations of hadronic showers. Technical developments will be necessary in addition as regards the electronic logic. Though it is impossible to plan a strategy today on this idea, the maintenance of activity at THÉMIS preserves the conditions for a very ambitious project.

I.2.3 THE CAT IMAGING DEVICE, CHOICE OF CHARACTERISTICS

The present project development depends mainly on the addition of an imaging device. Its characteristics have been chosen on the following basis:

- realistic extrapolation of the imaging technique by improvement of image resolution;
- a quality of cosmic observations which place us at least at the level of the best current or projected detectors;
- a construction that could rapidly be carried out, without any major problem, with a view to making the first observations in winter 1995.

This third point comes with financial as well as technical constraints. It would have been unrealistic to pretend to build a telescope which would be from the first the largest and most precise. The priority given to the high resolution has thus led us to consider a mirror diameter smaller than the Whipple's 10 m. In particular, it is very desirable that the whole telescope could be supported by one of the supports of the solar oven mirrors, so economising a complex mechanical piece.

The CAT project imaging device will include a 16 m^2 mirror, a size between the Whipple's 75 m^2 and CANGAROO's few 6 m^2 equivalents. This 16 m^2 mirror will be supported by a structure of about 5 m diameter.

The requirement of an optical system with small geometrical aberrations implies that the focal length must be at least as large as the diameter. The camera will thus be placed at a distance of 6 m. This choice fixes in turn the photo-detective surface to be built; assuming a shower image is longitudinally 20 mrad at most, the camera diameter must be almost 30 cm so that it covers more than twice this length.

Concerning the imaging resolution, the particular aim is to approach the specific dimensions of the images themselves. The zone of emission of the Cherenkov light ranges typically up to twenty metres around the axis of propagation (at least according to simulations since no device has yet been able to verify this); since the altitude is 6-8 km this corresponds to 2-3 mrad for the image width. The size of the pixels will be 1.9 mrad, a finer grain would doubtless not be more useful; we think that at least up to this resolution is of tangible interest. It is an improvement which is almost in the same proportion as between the 4.1 mrad for Whipple and 3.2 mrad for CANGAROO.

That the performance expected on the basis of this set of these characteristics will be at the level of the best current detectors is demonstrated in the simulations described below. Confidence in these estimations is supported by the development of Cherenkov imaging itself, and to a certain degree by the experience of these last years in the design of calorimeters beside large accelerators where tests and simulations can be married.

The way in which the various background noises interfere with the functioning of the high-definition camera is a significant problem which demands a good model for the showers themselves. In this regard, useful experience has been acquired by some of us who are associated with the Whipple group for the ARTÉMIS experiment. We have access to large data-sets; also, UV observation, specific to ARTÉMIS, brings a useful complementary "enlightenment": sky noise is considerably attenuated, which makes other types of noise (from nearby muons or collisions with the camera) likely to stand out and perturb, even in visible light, a detector such as the CAT imaging device.

With the imaging device placed at the centre of the existing device we will be able, for a certain energy range, to observe the same showers, to compare the results of analysis and also to associate on-line or off-line information coming from the ensemble, and perhaps to see hybrid strategies emerging.

I.3 Other projects in development at international level.

I.3.1 PROJECTS CURRENTLY BEING TESTED

- Whipple (USA): GRANITE, 2 telescopes with 70 m^2 of mirrors with 4 mrad resolution on the first telescope and soon on the second;
- CANGAROO (Australia) Japanese project: small mirror surface but ≈ 3 mrad resolution;
- CRIMEAN GT-48 GAMMA-TELESCOPE (USSR): A.A. Stepanian
- SHALON (USSR), Lebedev Institute (Nikolsky, V. Sinitsyna et al.)
- HEGRA (Canaries), German project: set-up of an imaging telescope

I.3.2 FINANCED PROJECTS

- HEGRA (Canaries): complement of 5 imaging telescopes with 4 mrad resolution on the central one and 7.5 mrad on the others;
- Narrabri (Australia), English project: imaging with several mirrors ... of high enough cost (3 million £...?).

II. High definition imaging device

II.1 Observational data.

Gamma and hadronic showers
Sky noise
Resolved stars
Monitoring of the telescope using stars
Energetic cosmic muons
  Ring images and monitoring luminosity
  Segmented images resembling γ showers
Cosmic collisions on the camera:
  other segmented images resembling γ showers, "darts"

II.1.1 GAMMA AND HADRONIC SHOWERS

The research into higher-resolution imaging is marked by the continuity of the steps in the development of the method. The first challenge was to subdivide the focal plane just enough so that the zones affected by a shower could be considered individually so as to increase the signal-to-noise ratio for the triggering. Concerning the analysis, the strategy had emphasised the measurement of the direction of the shower and it was not until after having increased the number of pixels that the power of the analysis of the shape of the images was realised. The shower simulations for gammas and hadrons have accompanied this instrumental evolution as well as providing its methodological basis. Fig. 1 shows a γ-shower image and a proton shower image obtained from simulations. At the same time, developing alongside the accelerators were calorimeters, various detectors which also are characterised by the observation of electromagnetic and/or hadronic avalanches; in their various generations, they have been optimised by simulations immediately validated by large numbers of tests with incident particles of known type and energy. The confidence so acquired in the possibility of precise simulation of these detectors extends to the case for atmospheric showers. It is in this environment that the instrumental bet must be placed, which for the CAT project is on high-definition imaging; rather than being a bet, it is a question of exploiting the margin that is available — according to MC simulations — between the intrinsic fineness of atmospheric avalanches and the resolution of the observing instrument.

II.1.2 SKY NOISE

The modifications of the detector towards a higher resolution will affect on the one hand the behaviour of night-sky noise and on the other hand the way in which this noise affects the triggering and the subsequent image analysis.

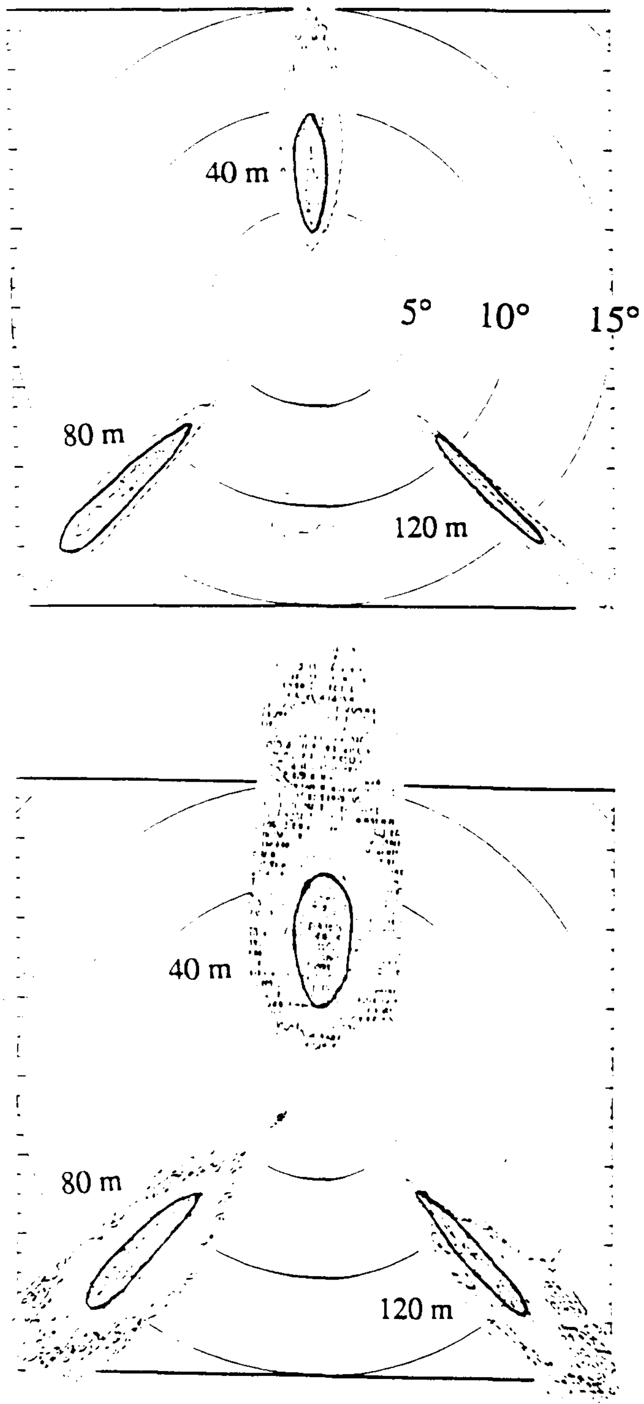

Fig.1 a) Images of three 2 TeV γ-showers with impact parameters of 40, 80, and 120 m respectively from the centre of the mirror;

b) Same for protons of the same energy.

To the first order, the higher resolution will decrease the noise per pixel, in proportion to the surface area of the pixels. For CAT, that is to say for an opening angle of 1.9 mrad per pixel and a 16 m^2 mirror, the noise per pixel is 0.1 / 10 ns. The immediate consequence is that in the duration of a few nsec, the typical duration of a coincidence, the probability of pile-up is low. The risk of parasitic triggering on the sky noise then depends primarily on the fluctuations in PM responses. The PM quality is thus very critical in order to obtain triggering on low-energy-threshold showers.

II.1.3 Resolved stars

Our attention has focused on the fact that the nocturnal noise — coming essentially from stars — is not solely composed of diffuse noise. From the small level of noise per pixel and the optical quality, all stars will be resolved up to about the 8^{th} magnitude. This implies few problems but opens the way to new monitoring possibilities for:

- telescope orientation,
- device luminosity,
- angular resolution of the optical system.

In particular, for the angular field of 30 mrad opening around the observing direction of the Crab, stars are distributed according to their magnitudes as indicated in Fig. 2 and in Table 1. The quoted magnitudes correspond to a wavelength of 430 nm, so in the neighbourhood of our region of sensitivity. In this table are shown also the effective rates of photo-electrons per pixel for CAT. Note that for an opening angle of 1.9 mrad per pixel and a mirror of 16 m^2 at the 8^{th} magnitude the rate of photons corresponds to two times the rate of diffuse noise, an acceptable level for the showers but still measurable. The Crab region is relatively unpopulated with bright stars; the advantages and disadvantages which result from the presence of stars will be more or less severe for other possible fields of observation.

This table shows clearly the various types of situation that, in general, will have to be taken into account:

- for high voltages, either shutting off in front of the brightest stars, or decreasing, or simply maintaining them;
- for the trigger logic, the probable exclusion of pixels up to the 7^{th} magnitude;
- finally, for the read-out, the importance of using all available data.

The use of an Alt-Azimuth type mount implies a rotation of the sky image on the focal plane during the tracking of a source, a rotation which becomes rapid when the observed source is near the zenith; the same stars stay in the field of view during the tracking of a source, however they do not stay in front of the same pixels. The over-illumination of certain PM's by the brightest stars must be taken into account as automatically as possible. It must be made possible to have frequent readouts of the PM's (independent of triggering events).

Table 1

Effect of stars of below the 9th magnitude in the neighbourhood of the Crab.

Magnitude	Number of stars in the field	Star noise (10^7 γe / s)
3	1 (ζ taurus)	200.
4	0	80.
5	1	33.
6	2	13.
7	4	5.
8	11	2.
9	56	0.8

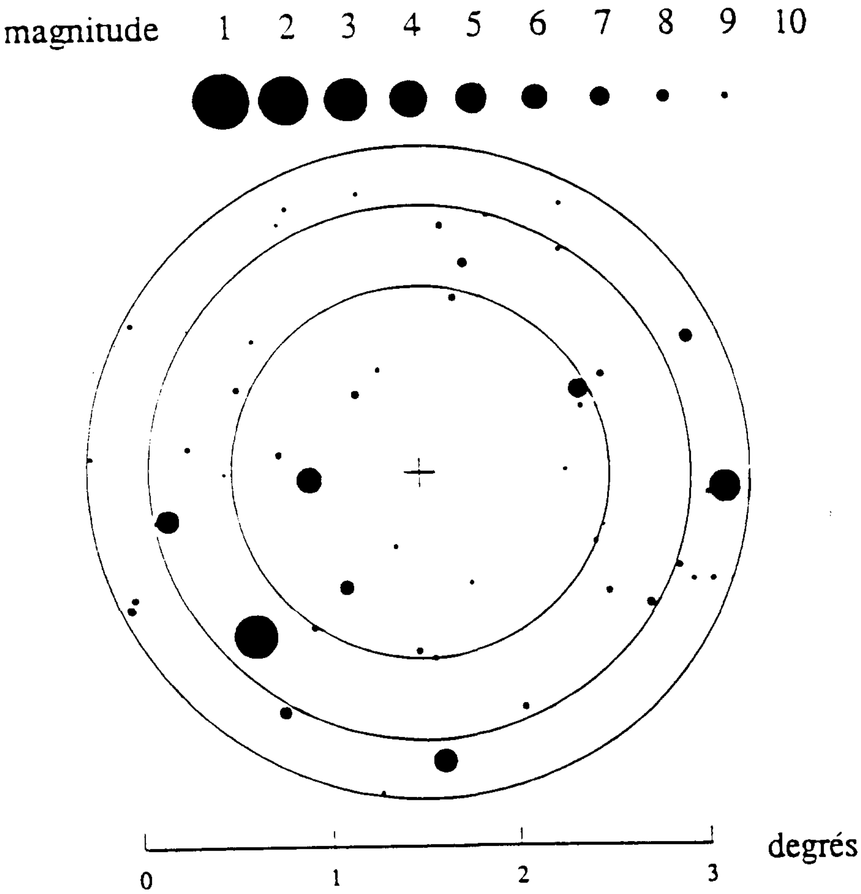

Fig.2 The sky in the neighbourhood of the Crab

Because of the high resolution, the starlight will be concentrated on a smaller part of the focal plane, giving therefore a greater area for shower images. This can facilitate the observation of certain regions of the sky which are rich in bright stars.

II.1.4 Monitoring of the telescope using stars

The previous disadvantages are compensated for by the ease with which individual images of certain stars can be obtained. This appears to constitute a new and essential element, allowing the realisation of various continuous controls, such as luminosity monitoring and more important yet, the monitoring of the pointing.

The monitoring of the telescope pointing by the observation of stars in the camera presents the enormous advantage of placing in direct relation the sky field and the detection plane of the shower images. This monitoring can doubtless be realised in a continuous way throughout the tracking of the source. The reading of the camera can proceed, independently of triggering events, while optimising the parameters which can be changed (such as duration of integration of charge and readout frequency).

The observation of individual stars and the measurement of the received photon flux will provide a useful estimation of the collection efficiency for photons. During a night of observation, the atmospheric transparency is the most likely variable due to the presence of possible clouds which will be put under surveillance in this way. From one night to the other, the state of the mirror might induce variation. Over longer periods, the mirror or the PM efficiency could be the cause of variations.

The measurement of the transit of a star from one pixel to another will provide a profile of the telescope's angular resolution. This process is in widespread use; it will be possible here to use it as a permanent tool.

II.1.5 Energetic cosmic muons

II.1.5.1 <u>Ring images and monitoring of luminosity</u>

This monitoring of the rate of detected photons by the measurement of a few "witness" sources will be complemented by the observation of muon rings. On the Whipple telescope, UV observation with the ARTÉMIS experiment has established presence of these "ring images" which are produced by cosmic muons above an effective threshold of $\approx$ 8 GeV falling on the mirror or in its immediate vicinity. Whereas at Whipple these rings could be seen only in UV light which favours the observation of nearby sources of emission, with CAT these ring images will be above noise level even in visible light; as they contribute $\approx$ 10 γe per pixel these muons will be normally taken into account in the triggering. An annular image is immediately identifiable provided it spreads over about 15 pixels, which corresponds to cases of direct collisions on the mirror; with a rate of $\approx$ 0.2 Hz. These cosmic muons will contribute to the monitoring of the collection efficiency for photons. This monitoring is not concerned with the atmospheric transparency (except for a few hundred metres immediately above the detector) and so is complementary to the method provided by the stars.

II.1.5.2 Segmented images resembling γ showers

The annular images reduce to short segments when the impact point of the muon is further than several times the mirror radius. For segment lengths of typically between 3 and 6 pixels, corresponding to impact distances between 3 and 6 times the mirror radius, these muons are at risk of being confused with low-energy γ-shower images. The rate of muons for this impact area (with a 5 m diameter mirror) is a few Hertz. Of course, these effects show random orientations but the criteria on the shape explained in II.4.2 will reject them effectively.

II.1.6 COSMIC COLLISIONS ON THE CAMERA: OTHER SEGMENTED IMAGES RESEMBLING γ SHOWERS, "DARTS"

Through direct interaction with the PM's, cosmic particles are likely to generate filiform and rectilinear images of varying lengths. For the Whipple telescope, these effects have been particularly well observed by the UV camera thanks to the smaller sky-background noise. For about 80% of these "darts", the efficacy of a veto realised using a set of scintillating counters placed around the camera can be demonstrated. The number of photons per pixel is in general much higher than for a shower with small lateral extent. Since the darts are much more numerous than showers of low intensity, their susceptibility of confusion with low-energy showers remains a problem. Their rate depends on the PM's used, on their mass and their shape; this rate is ≈ 0.3 Hz at Whipple. A study will have to be carried out as soon as possible with the PM's that will be chosen to equip the camera.

II.2 Technical choices for the imaging device

II.2.1 THE TELESCOPE:

MECHANISM, MIRRORS, AND TRACKING OF COSMIC SOURCES

II.2.1.1 General description

The general organisation of the mechanics will look very much like the Whipple telescope, essentially due to similar constraints leading to same solutions. For reasons of cost, the mirror itself will consist of discrete elements all with the same radius of curvature. This entails their arrangement on a spherical frame whose centre is occupied by the camera: the Davies-Cotton design. Seen from an axial position, the components are tangential to a parabola with the camera at its focus but, for each ring, the parabola is different. Such a device is not isochronous, and the isochronic defect varies as the square of the opening; the maximum divergence between the centre and its circumference is in our case 1.6 ns.

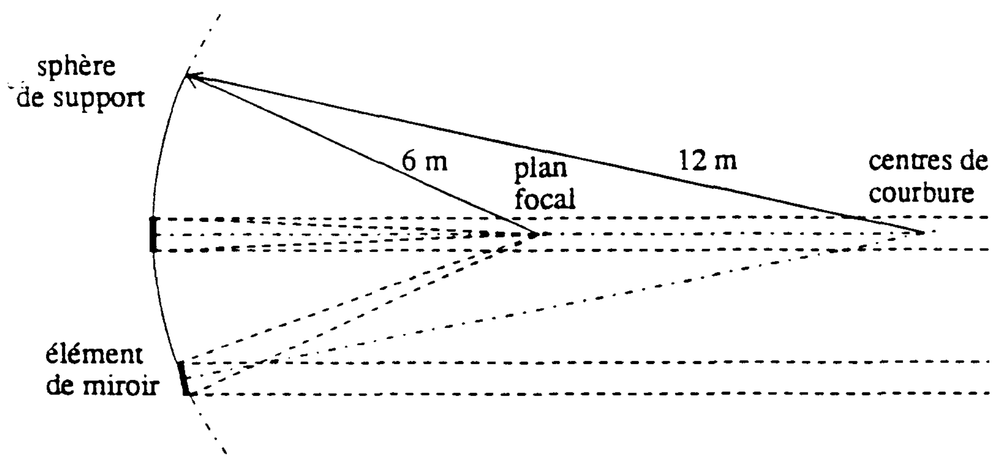

Fig.3 Diagram of the principle of the Davies-Cotton mounting

The Davies-Cotton arrangement of the mirror components is shown in Fig. 3. This is a scale drawing, preserving the relative positions and angles; the angular shift between the mirror elements and the arc of the supporting sphere can be seen. In comparison with an arrangement with a parabolic frame, the isochronism would improve but, beyond 1° from the optic axis, the geometrical aberrations would become severe.

The mount will be of the Alt-Azimuth type as has become usual since computers permit the tracking to be achieved as easily as with an equatorial mount; in fact it will be a mount taken from one of the THÉMIS heliostats.

The diagram of the ensemble is shown in Fig. 4.

Regarding three secondary points we will innovate:

1) The arms supporting the camera will be supported directly on the counterweight set, so avoiding the addition to the strains which the structure carrying the collection surface will undergo;
2) The electronics will be mechanically bound up with the moving part of the telescope and installed partly in the camera and the partly in the neighbourhood of the counterweight; so minimising the weakness of the numerous interconnections. This also gives some protection from electronic noise by placing the ensemble in the same Faraday cage.
3) The telescope will be put under a shield outside operating hours, as is desirable for a device which is both relatively compact and highly precise.

Essentially, the specifications of the CAT telescope are defined by the numerical values of the chief components:

– pixel size	s = 1.25 cm^2 (linear size 1.9 mrad)
– collecting surface	16 m^2
– focal length	6 m
– angle of field of view	± 25 mrad

The first two terms in fact reflect our aims ... limited only by the financial constraints. The focal length is at least 6 m so that the geometrical aberrations do not encumber the resolution of the pixels. The angle of the field of view is imposed by the size of the shower images.

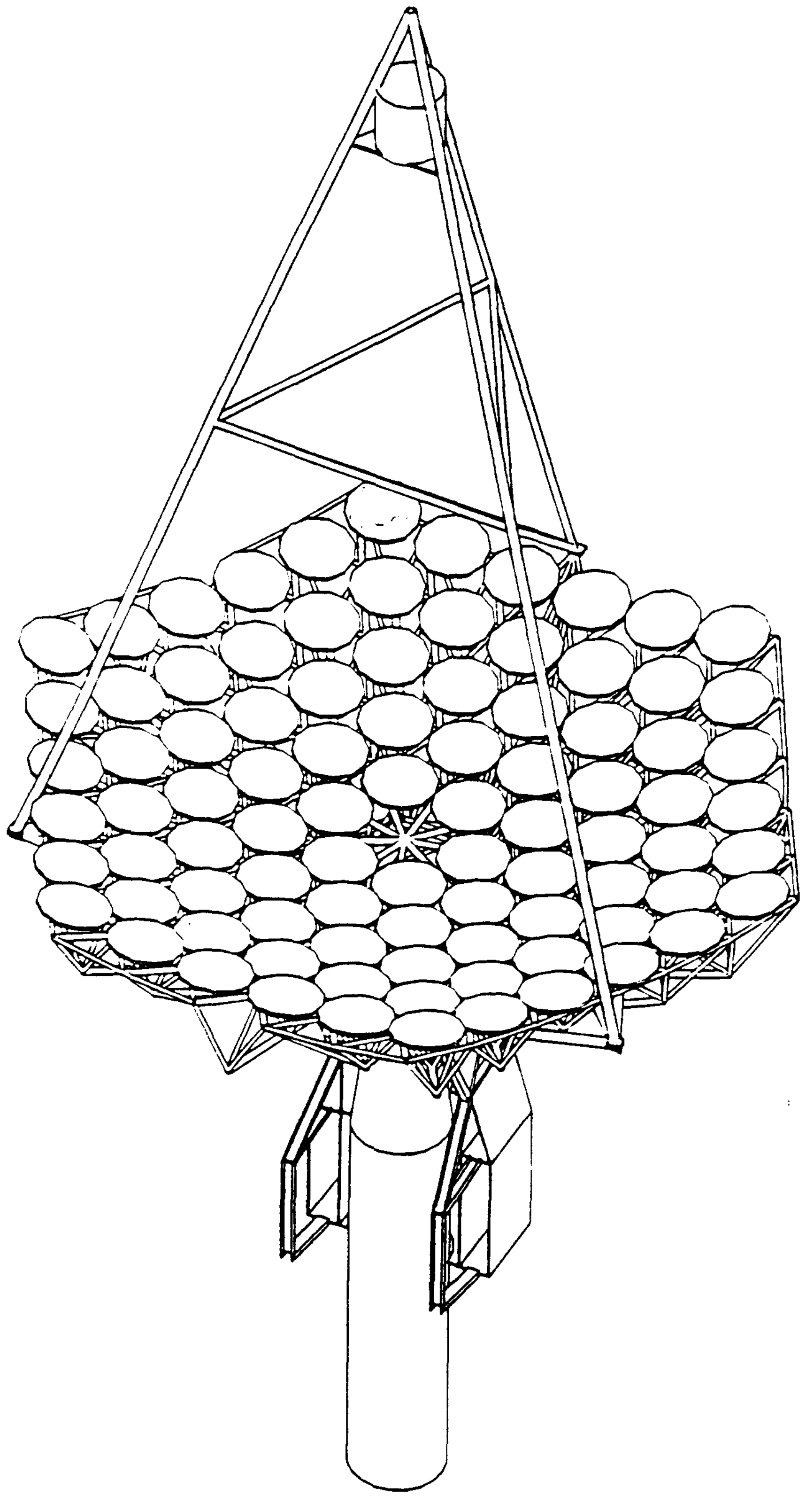

Fig.4 View of the telescope ensemble

II.2.1.2 The collection surface

II.2.1.2.1 Dimensions of elements

The size of the mirror components is limited partly by manufacturing constraints and mechanical stability and also by the geometrical optical aberrations. The decision made is for 500 mm diameter, which corresponds to 90 mirrors arranged in 5 rings. The central component, uncounted, is left free for test devices. The collecting surface is thus

$$90 \text{ elements} \times \pi/4 \times (0.5\text{ m})^2 = 17.8\text{ m}^2$$

which taking reflectivity into account corresponds to about 16 m^2 effective area.

The shape of each element will be circular, which is preferable to square or hexagonal shapes which though better for maximum collection are susceptible to larger geometrical distortions in their corners. The free spaces will be useful for access for adjustments (the mirror zone can scarcely be reached through the framework).

II.2.1.2.2 Materials and surface protection

The reflectivity of the mirrors must be as high as possible in a wavelength region from 300 to about 550 nm. Below 300 nm absorption of the light by the atmosphere becomes significant, above 550 nm background noise from stars becomes predominant. From a technical point of view, the difficulties lie in the smaller wavelengths for the PM windows and the mirrors; the passage of the light through glass must be avoided. Whether the mirror is glass or aluminium, the aluminium reflecting surface must be on the front face, which is more fragile than a mirror of back-aluminised glass.

The constraint introduced by the possible deposition of dew on the reflecting surface is a little known problem. The materials from which the mirrors are made constitute one of the parameters of thermal equilibrium which itself affects condensation. Front reflectivity, favourable to radiative exchanges with the night-sky background, slows the cooling of the face and so can retard or supress the effects of condensation. It is hoped that this favouravble situation will suffice; these test must be proceeded with in due course.

The protection of the reflecting surface will be accomplished by transparent anodisation of the aluminium. The optimal thickness of alimunium is a half wavelength of the reflected light, so (taking account of the index of aluminium) it is about 100 nm for a maximal reflectivity near $\lambda \approx 400$ nm. The layer will be fairly absorptive for $\lambda > 600$ nm, which would in general be a prohibitory handicap for astronomical observation but is favourable for us since the noise from stars becomes preponderant in this region (the mirror becomes a blue filter). This quite easily performed technique is currently used by the American Fly's Eye and Whipple Observatory groups, with lifetimes of more than two years for mirrors permanently subject to bad weather.

II.2.1.2.3 Mirror construction

Two possibilities are currently being explored in industry, taking into account a three-year study of the repair of the mirror in the military oven in Odeillo:

- an aluminium honeycomb sandwich, of 20 mm total thickness, with the optical face machined with diamond on a numerical automated machine and protected by a transparent anodisation treatment.
- glass 10 mm thick, machined, polished, and aluminised in a vacuum, with same type of anodisation protection.

The imposed tolerances are ± 1' (i.e., ± 0.3 mrad) defined as the deviation of the direction of the normal at each point with regard to the theoretical direction. This tolerance is well defined by saying that 80% of the light must fall within a 1 mrad spot. This second criterion includes scattering effects.

The choice will be made mainly on the basis of the cost and the examination of samples.

Note that independently of these considerations there is an argument in favour of glass, due to its higher resistance to bad weather (a periodic retreatment is anticipated).

The aluminium option will allow, on the other hand, without extra cost, the use of two values of curvature to reduce the time dispersion by approaching the parabolic shape. The deviation would thus be brought below a nanosecond. The surface anodisation treatment does not require treatment under vacuum, which would pose difficulties for a honeycomb structure.

II.2.1.3 Mechanics

A first study of the mechanical assemblage has been done with simulation tools which allowed a first draft taking into account explicitly the criteria of stability; a draft sufficiently detailed for submission to a manufacturer who has given us a cost bracket.

The piece constituting the axis of the telescope, together with the motors, encoder and controllers, will be taken from one of the heliostats of the solar power-station.

The platform currently supporting the heliostat mirrors will be replaced by a very rigid mechanical piece forming the basis of the construction of the whole telescope. We explain below these three elements which are fixed to it independently: the structure supporting the mirrors, the structure supporting the camera, and the counterweights.

II.2.1.3.1 Mirror structure

This will be a reticulated structure made in welded steel sections. The geometrical ratio of the connections is chosen as a function of the geometrical ratio of the mirrors. The inertia of the sections is chosen to limit deformations due to variations of the angle of the telescope according to the coordinates of the observed source or during tracking.

Only the angular effect at the level of each mirror is taken into account. This must not go over ±0.1 mrad.

Each mirror is fixed at three points, two of which can be adjusted; these adjustments must be performed via the front face.

II.2.1.3.2 Structure of the camera support

The telescope angle is capable of varying between 90° (zenith) and 0°. It follows that a large variation in torque is introduced by the weight of the camera which is situated 6 m from the mirrors. It is expected that the camera will weigh 90 kg (not including the weight of cables spread along the supports).

The design of the camera structure, so as not to apply force on the mirror structure, avoids any contribution due to this torque on the mirror structure.

The displacement of the camera with respect to the mirror frame of reference does not imply any deterioration of the shape of the image. Moreover, these displacements will generally be continuously monitored by the observation of stars up to almost the 7th magnitude, which are sufficiently numerous that there are several in the camera field whatever the observed sky zone. Thus the tolerance on the relative displacement of the camera is dependant mainly on a criterion which is not very restrictive for good exploitation of the field of view. In the most usual case of observation of a point source, the source must not go further than 1-2 cm from the centre of the field. This criterion appears to be less constraining than the minimum conditions of mechanical rigidity.

II.2.1.3.3 The counterweight

It is envisaged that the counterweight function will be implemented with two symmetric locations on the same structure for the placement of the necessary masses, in such a way that motion is not blocked by the column. Instead of purely passive masses, these locations could be used for electronic racks. This zone of the installation would become active and must be easy to access, above all when the telescope is in its shelter.

II.2.1.4 Auxiliary devices

II.2.1.4.1 The shelter

The difficulty in guaranteeing a sufficient weather-resistance of all telescope elements has led to the design of a shelter. The site is exposed to tornadoes from which the solar power-station has already suffered. The use of a shelter will certainly entail extra cost. The savings that it will bring about are not easily calculated, as they depend on the one hand on hazards and on the other on increased facilities for the building and maintenance tasks that could then be done indoors. The distribution of staff on the site will be more cost-effective. Moreover, the building of an orientable ensemble of electronic and mechanical parts would not have been conceivable without this shelter.

The solution decided upon consists of a fixed shelter and a telescope which is made mobile by placing the central column on a trolley (Fig. 5). The shelter presents a large surface to the wind,

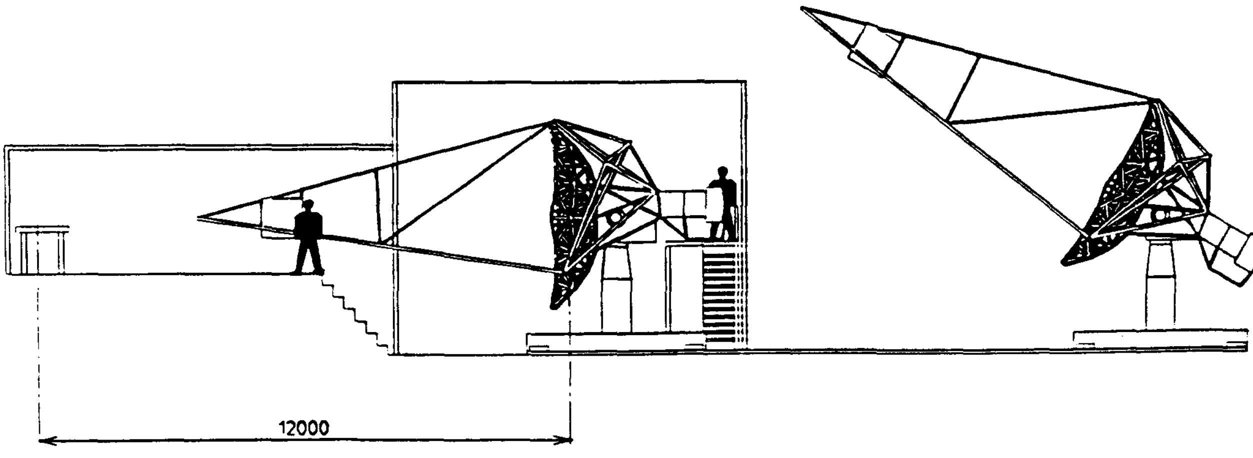

Fig.5 The telescope in parked position (left) and in observation position (right)

and it is easier to link it to the ground than to have it move. The shelter will consist of a semi-cylindrical structure of 5.5 m radius placed on a concrete flagstone. The trolley will move on two rails and will be positioned on the observation area using two jacks.

II.2.1.4.2 Albedo protection

During tracking, the camera is exposed to parasitic light reflected or diffused by the ground, and as such more severe since the optics of the system have a small opening angle. This albedo effect is particularly dangerous when the ground is covered with snow; yet the better observing periods are in winter since the nights are longer. To avoid this background noise, masks are placed, as shown in Fig. 6, in such a way as to cover all parasitic angles of view. This very necessary device will be constructed so as to minimise as much as possible the wind loading, but the sheltering of the device in bad weather will permit us to lighten these building constraints.

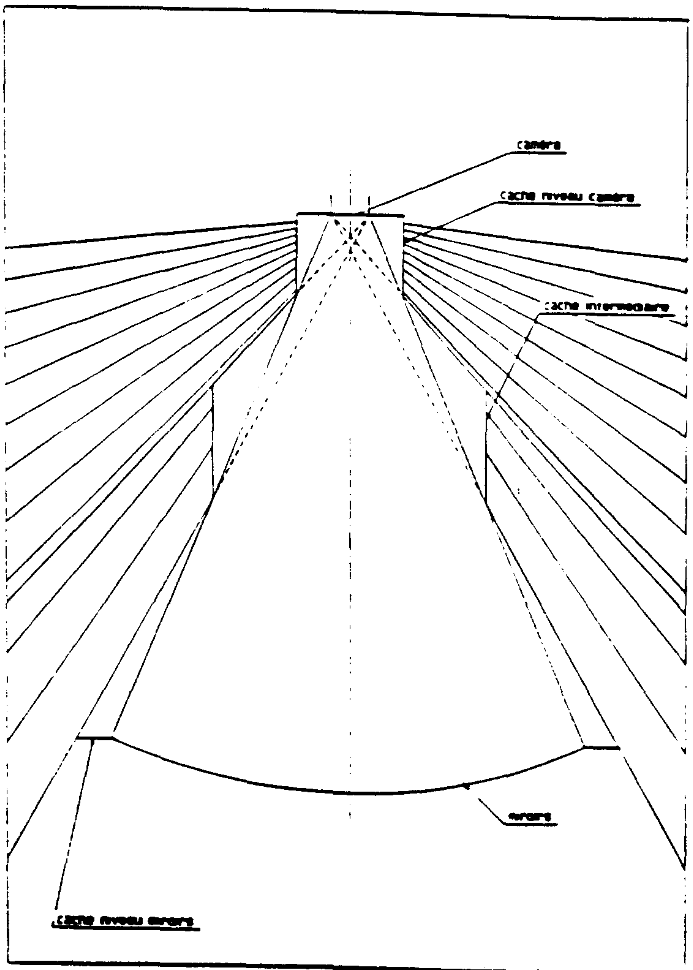

Fig.6 Anti-albedo device

II.2.1.4.3 Lightning protection

It is known that several cosmic-ray experiments have suffered great damage due to lightning in recent years. The possibility of enclosing in a continuous circuit — conceived as a Faraday cage — all the elements constituting the camera and the electronics appears to us to give a certain amount of protection against such catastrophes. The link between the control room and the camera is made with fibre-optics. Nonetheless, the distance of about ten metres between the camera and the counterweight area where most of the electronics is found leaves a certain vulnerability in this Faraday cage. A very low resistance electrical link between the two regions of the camera and the counterweight must be made. This protection is not exclusive of other approaches to the lightning problem for which it is necessary to consult specialists in these problems.

II.2.1.4.4 Mirror adjustments

The mirror is a mosaic: the proper orientation of each element must be adjusted and verified. The frequency of these realignments is difficult to forecasted as it will depend on the structure's stability over time. This uncertainty requires that the alignment process be reasonably easy and fast and that it should be possible in daylight.

The verification will be done using a CCD camera and a light source placed on the optic axis of the telescope near the centre of curvature; i.e., at a distance 2F from the mirror. At the focal plane of this camera the images of all the mirror elements will be simultaneously visible (or part of these elements for the first ring which is partially masked by the camera). The effective position of the images constitutes a measurement of alignments which can then be analysed on-line by a processor. The eventual corrections will then be made manually using adjustable supports accessible from the front side.

This step demands that the telescope will be positioned with its axis horizontal. The alignments will not then be verified for every observational position, so it is important that the mechanical structure is such that the distortions during tracking stay within the tolerances.

II.2.1.4.5 Cosmic tracking

From the point of view of the mechanics and electronic servos, the tracking of a cosmic object will be accomplished using the existing resources re-used from the solar power-station.

The software will be either a modification of that of ASGAT or probably that of THÉMISTOCLE.

Real-time monitoring will be accomplished by the observation of stars in the field of view of the camera (see II.1 *Observational data, II.1.1*). Except in the case of an anomalous shift, this information will not take an interactive part in the tracking: it will be sufficient to use it off-line.

This monitoring has the enormous advantage that it directly concerns the positioning of the measurement plane. It demands only that the whole structure track without jolting, the necessary absolute precision staying at about a few mrad.

A CCD camera having a field of view of the sky greater than the telescope will be mounted on the mirror. This camera will not have to ensure precise monitoring of the tracking because this monitoring should be itself corrected for displacements between the optic axes of the two systems; its rôle will be to allow a direct verification — by identification of the brightest stars — that the telescope orientation is to the first order in the region of observation.

II.2.2 THE CAMERA: THE PM'S AND THEIR OPERATION

II.2.2.1 Choice of PM

II.2.2.1.1 Criteria for choice

The camera must provide a very fast image of the shower while avoiding that this "snapshot" be crowded with too many parasitic photons. The PM's provide not only the arrival time, defining the trigger, but also the image shape based on the distribution of impact points in the focal plane. Having as the first objective the observation of showers of lowest possible energy, so with very few photons, we aim to exploit to the maximum the information received by the mirror.

The characteristics that we have chosen for the imaging device, which are presented in §I.2.3, have obliged us to find a PM satisfying several criteria:

- small geometrical obstruction, such that each PM corresponds as well as possible to the size of one pixel
- a fast response time with low dispersion
- a single photo-electron response as well defined as possible.

This last point, which characterises the "photon counter" PM's, is necessary mainly to allow us to trigger on the basis of a selection of responses at the level of only a few γe's; thus for a threshold of 4 γe, the sky noise which can reach the 2 γe level on the typical time of a coincidence must only rarely stimulate a response at this level of 4 γe. As for the reading of the charges of each pixel after triggering, it must give as true an estimation as possible of the number of γe's: invariably for the case of weak showers, maximum advantage must be taken of the small statistics of the available γe's, because a good analysis of the image shapes allows both measurement of their orientation and the separation of γ-showers from the background noise of hadronic showers.

II.2.2.1.2 The Hamamatsu 1635-02 PM, Ø = 3/8"

The pixel density required, and thus the small PM obstruction required, has limited us practically to one supplier, Hamamatsu. The "pencil" shape PM's are manufactured with a diameter of 3/8". The range requires a "photon-counting" PM whose amplitude distribution for a single γe is Gaussian of width 0.4 γe. We have been able to verify this behaviour and have shown that spectral response for a few γe followed perfectly well the distribution expected by convolving a Poisson distribution (for the number of γe) and a Gaussian distribution of width $0.4\sqrt{n}$, where n is the number of γe (Fig. 7)

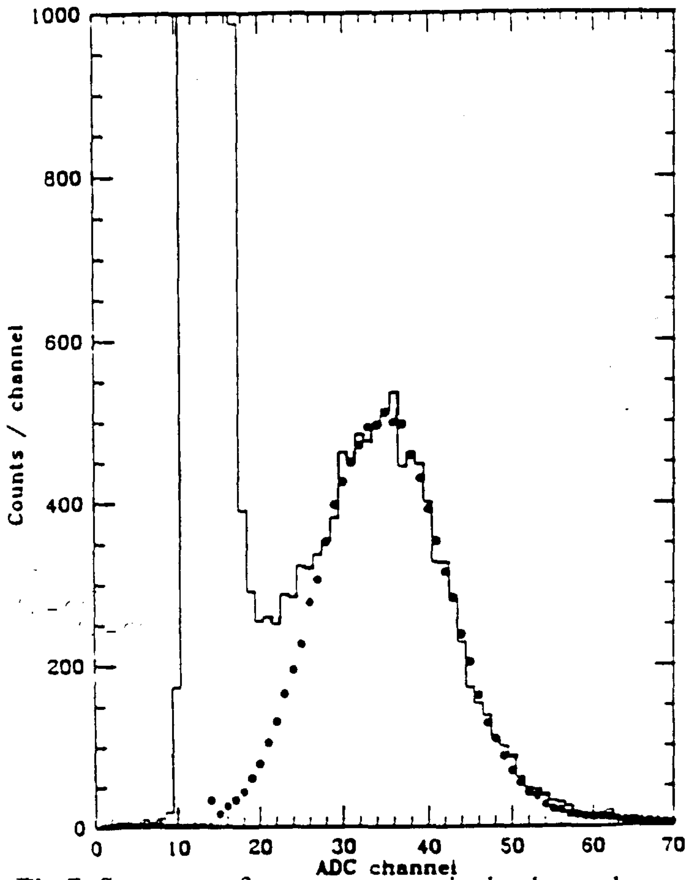

Fig.7 Spectrum of responses to a single photo-electron

This PM also has a very fast response time, allowing us to look at coincidences of the order of a nsec which correspond to the order of magnitude of the dispersion in the arrival time of photons of one shower.

II.2.2.1.3 Quartz photo-cathode windows

The maximal exploitation of the shower photons lead us ultimately to use PM's with UV glass so as to preserve good detection efficiency down to just below 300 nm. Moreover, the results obtained recently by the ARTÉMIS group establish that moonlit nights can be usefully exploited for the study of γ-sources using UV light detection (with additional filtering of the visible light).

II.2.2.1.4 Simulations

The simulation of the detector incorporates a model of these PM's response (and of the associated electronics), in order to estimate the performance of the whole as regards the trigger and the shape analysis. This same analysis tool can be used for a comparative evaluation of other choices of PM.

II.2.2.1.5 Number and cost

The field of ± 17 mrad is covered by 1635-02 PM's of Ø = 3/8";i.e., about 10 mm (spaced by 2 mm). This corresponds to 282 PM's in the central zone (shaded) in Fig.8.

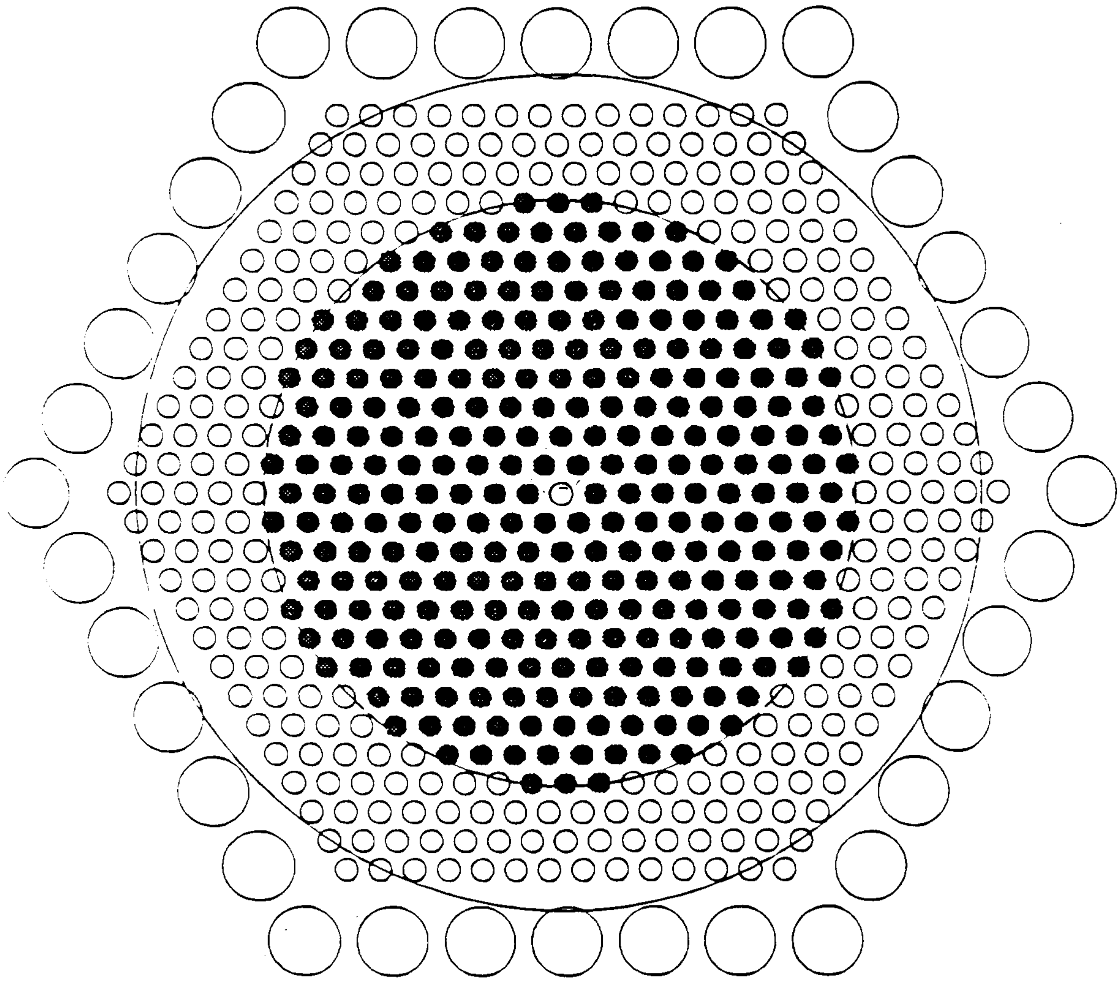

Fig.8 Positions of the PM's the camera. Shaded: the trigger PM's.
The two circles are drawn at 17.5 and 25 mrad respectively.

For the external zone of the focal plane, between 17 and 25 mrad, if the use of the same PM's constitutes the best solution, nonetheless we anticipate various other solutions of lower cost. The diameter can either be increased from 3/8" to 1/2", thus decreasing the number, or else the least efficient PM's in terms of single γe counting can be used. The principal economy would be the one relating to the lesser-quality PM's.

If the decision is for a homogenous set of small diameter tubes, they will be 547 in number.

In any case, before opting finally for a hybrid solution, it would be prudent to verify by careful simulation what it will cost regarding loss of performance for the observation of showers.

II.2.2.2 Array of PM's

The PM's will be arrayed as compactly as possible, in a hexagonal distribution and practically in mutual contact. The arrangement of the ensemble of the camera is shown in Fig.9.

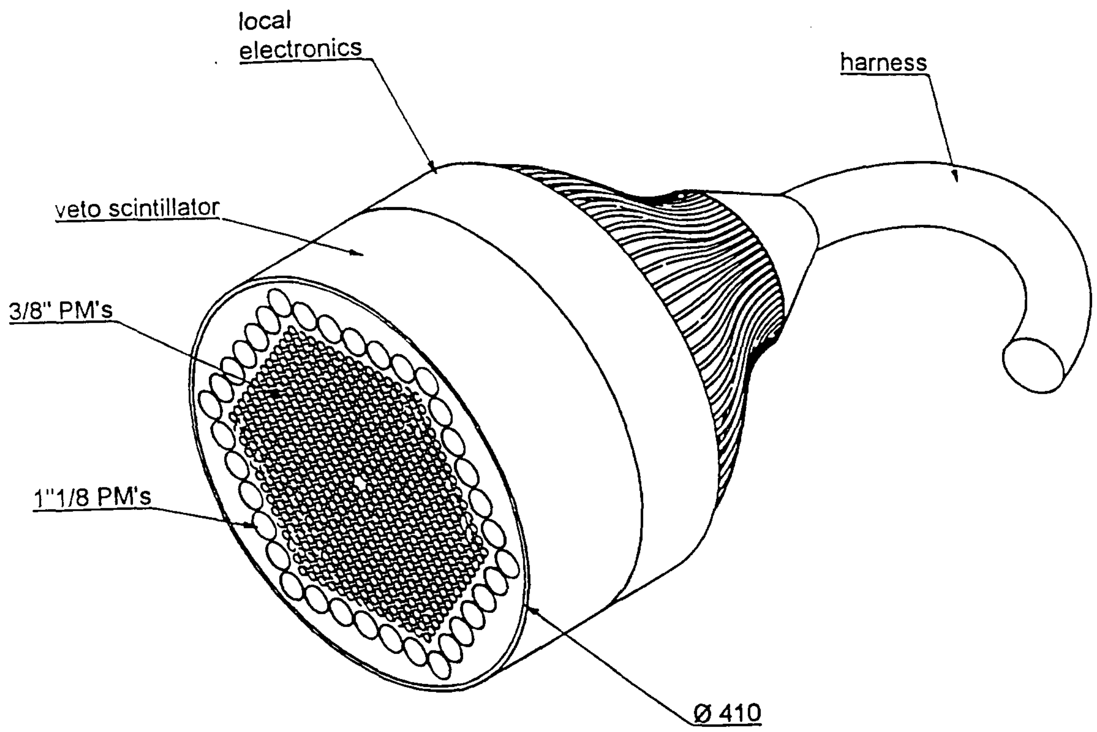

Fig.9 The camera box

II.2.2.2.1 Collecting cones

In this very compact arrangement, the dead space between PM's remains, however, of the same order as the sensitive surface. It is in principle possible to recoup the photons which fall outside the photo-cathodes using conic collectors. The relatively small opening angle of the telescope allows a collection efficiency close to 100% (which is not the case for the Whipple telescope where the opening angle is about twice as great). These cones will be pierced in a sheet of isolating material, the reflecting surfaces being obtained by applications of aluminised mylar to the front face, the aluminium being itself protected by a thin film SiO. This method is currently being tested at Whipple.

II.2.2.2.2 Veto scintillator

The camera will be equipped with a set of scintillators constituting a veto against the cosmic particles interacting directly on the PM's or the immediately surrounding materials. This type of effect is known to give rise to images that can be confused with γ-showers. The scintillator will be placed so as to intercept as well as possible the charged cosmic particles. It will consist at a minimum of a cylinder surrounding the PM region. It would be judicious to insert another cylindrical scintillator inside the PM region, for example at the level of the transition zone, towards 15 mr. The bottom of the camera will also have to be covered by a veto scintillator.

II.2.2.2.3 Mounting of the PM's in the camera

The PM mounts, which as well as ensuring the passage of supply and signal cables must allow the possibility of access, constitute a challenge for their mechanical implementation. Note that the regularity of the hexagonal mesh will have to be ensured, but that it is not necessary to control in too regular a fashion the absolute position of the PM's (with regard to some frame of reference). Indeed, according to the camera orientation, the camera will undergo displacements with respect to a frame linked to the mirror. The permanent measurement of the position of a few stars in the field of view of the camera will permit us to counteract these uncertainties.

II.2.2.3 High voltages and gain controls

II.2.2.3.1 Preliminary calibration of gains

The individual characteristics of each PM will have to be calibrated and carefully recorded before assembly. The gains in particular are likely to have large deviations even for those from the same series.

Tracking of the gain stability will be possible during data recording, by the process of frequent readings of all lines outside event triggers (this reading will be done with a longer integration time than for events).

II.2.2.3.2 Individual high voltage supplies

To maintain a gain homogeneity of the order of a few percent over all the camera, the high voltage of each PM must be permanently controlled with a precision of the order of almost 10^{-3}. This presupposes individual high voltage supplies that can be controlled by computer. We envisage the use of a device recently developed by the Kiel group for the HEGRA experiment (Ref. 12) based on a common supply (or by sector) but modulated for each PM in a range of about 300 Volts by a resistive bridge controlled by a photo-diode; the system is servoed so that the output voltage on each line is stabilised with a low reference voltage to a precision of the order of a Volt. A central unit will have to continuously generate these low level voltages for all the PM's. These levels will be first defined from calibrating values. A dynamic adjustment is anticipated by modifying the calculated values, as a function of the PM behaviour in real time.

The modulation of voltages in a range of about 300 Volts could be insufficient either because of the light of a bright star or the pathological behaviour of a PM, an eventuality which cannot be ignored given their large number and difficulty of access. The high voltage distribution device will have to include a switch on each line that can be controlled by computer.

II.2.3 THE ELECTRONICS: TRIGGERING AND READING OF EVENTS

II.2.3.1 Functions and performance

The electronics linked to the imaging device can be divided into four functions:

- The validation of the signal of each pixel
- The triggering logic of the imaging device acquisition
- The treatment of the signal of each pixel
- The data reading and its storage in the central processor.

The required performance of these electronics comes essentially from aims and constraints linked to scientific observations such as we have presented in II-A. To satisfy them we have chosen fast PM's, measuring at the photo-electron level; the section on the camera gives a detailed description of the performance of these PM's. The essential qualities of the electronics will be:

- the rapid processing of the signal
- the dynamic range.

II.2.3.1.1 Speed

1 in the validation of the signal

The contribution of the sky background noise is inversely proportional to the time of coincidence. This time can in principle be very brief, of the order 1 to 2 ns, because the photons from showers are approximately synchronous and the mirror introduces a maximum dispersion of 1.6 ns. In order to exploit to the fullest the speed of the shower signals we will use comparators that impose no choice on the width of the profile and so should allow us to obtain very low coincidence durations (< 5 ns).

2 for the measurement of the charge of the signals

We want to eliminate as much as possible the contamination of our signal by photons from the sky background. For this we must integrate the charge on as narrow a gate width as possible, compatible with the width of our signals. By taking a background sky noise of 0.2 γe / 10 ns (a very conservative hypothesis) we can calculate the range of contamination for ≥ 1 or ≥ 2 γe in a given gate width:

Pile-up Rate		Gate Width
≥ 1 γe	≥ 2 γe	
63 %	26 %	50 ns
33 %	6 %	20 ns
18 %	1.7 %	10 ns

To analyse 200 GeV showers, comprising not more than a score of γe's, it is important to be able to be able to exploit the pixels up to a minimal level of 2 γe. From the numbers in the table, limiting the gate interval to 10 ns will guarantee an image with little pollution from sky noise. The PM's under consideration are sufficiently fast (FWHM < 2 ns) that practically all the charge is contained in such a gate. No ADC multiplexer on the market has such a small width. The use of fast analogue gates must allow the elimination of almost all sky photons that do not arrive in time with their opening.

II.2.1.3.1 Dynamic range

We have decided to be able to measure single γe's. On the other hand, we want to cover as large a range as possible, towards the high energies of the THÉMISTOCLE data. From the Monte Carlo simulations, a shower of 10 TeV can deposit of the order of 500 γe in one pixel.

We want to measure a charge between 1 and 1000 γe.

II.2.3.2 Implementation

II.2.3.2.1 Triggering electronics

a) validation of the signal

This will be done by comparators whose threshold will be chosen to be as low as possible. The limitations will be given by the rate of random coincidence produced by the background sky-noise, at the level of our triggering logic. With a hypothesis of Poissonian noise and for a signal of 2 ns width and a 16 m^2 mirror, we expect an individual count rate of the order of:

Individual rates (Hz)	Level of comparator
$< 5 \times 10^{-2}$	6 γe
$< 10^{2}$	4 γe
$< 5 \times 10^{3}$	3 γe
$< 4 \times 10^{5}$	2 γe

It seems realistic to fix the comparator threshold to 4 γe. The minimum threshold of these is about 10 mV. We must therefore adjust the amplitude of the PM signals corresponding to our threshold, so that they pass this minimum value. Starting with the reasonable hypothesis of a PM gain of about 10^6, a photo-electron is equivalent to 160 fC; this charge carried by a pulse of width 2 ns gives an amplitude of the order of 4 mV. Therefore, it is necessary to put a large-bandwidth amplifier on the trigger line. We will not be constrained there by a saturation effect at this level.

b) triggering logic

We anticipate a strategy based on statistical considerations of the arrival of photons at the mirror. We do not envisage at the moment the creation of an implementation algorithm based on a hypothesis of image shape. This would force us to treat the information coming from several pixels and so would slow down the triggering decision. It is perhaps conceivable to use it at a higher level. The trigger will consist of a majority coincidence, requiring that n pixels be simultaneously above the comparator threshold.

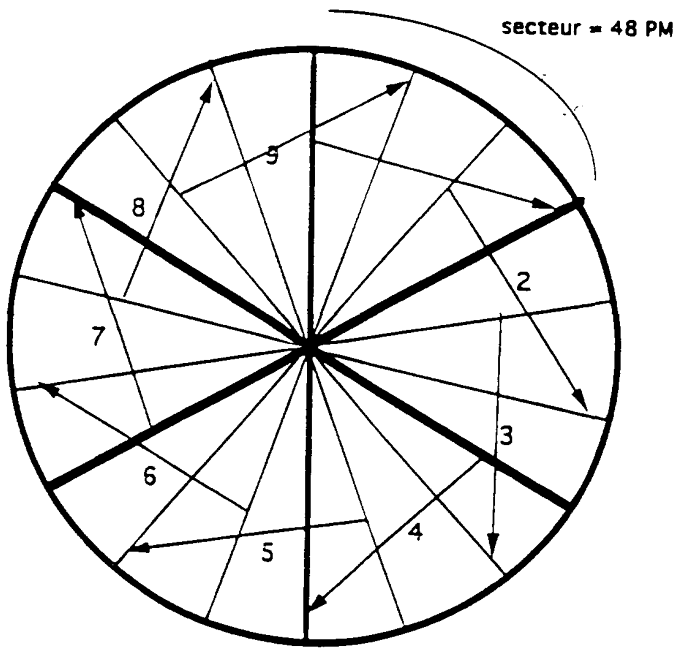

Fig.10 Segmentation for the trigger

Only the PM's situated inside a circular region of radius corresponding to ≈17 mrad will be used for the trigger. This choice is predisposed to the observation of a point source in the centre of the field of view. As we saw above, the rate of individual counts for each line being fairly high, a combinatorial factor must be avoided which would lead to an undesirable rate of random events. For this we divide the camera into 9 angular sectors (48 PM's) with an overlap of 16 PM's from one sector to another (see diagram in Fig. 10).

To reject more efficiently still the parasitic triggering of the sky noise, we foresee the addition to the majority condition of the extra condition that one of the pixels of the image be typically double the majority condition. This condition is normally satisfied by a shower, while dividing the rate of accidental events due to sky noise by 10^5. This condition will be implemented by adding a second comparator to each line so as to define a low threshold and high threshold..

To keep a maximum flexibility, we anticipate the possibility of two types of trigger:

- n1 pixels > low threshold
- n2 pixels > low threshold AND 1 pixel > high threshold.

The study of the simulations will help us to define the optimal configuration taking account of the physical objectives that we will have chosen.

c) Sketch of the implementation of the triggering electronics

For technical reasons we propose to implement this summation in two steps:

A first stage of summation on 16 lines (VME card), each receiving an amplified analogue signal; 18 cards (T1) will be necessary to treat all the pixels participating in the trigger.

At the level of this card, we envisage outputs sent to a counter, with cyclical reading on all lines.

A second stage of summation with threshold expressed in number of lines triggered, will be implemented on a single card (T2) (see diagram in Fig. 11).

The majority condition will be done in an independent fashion for each sector, that is to say on the analogue sum of the outputs of three adjacent T1 cards.

To implement the first trigger above, it remains to perform an OR on the 9 sectors. In the same way another logic unit will allow us to implement the second type of trigger including a high threshold by sector (Fig. 11).

The formation time of this trigger will be less than 30 ns.

We will study the possibility of placing these electronics in the immediate neighbourhood of the PM's, in the camera. The alternative would be its installation in a VME crate placed in the counterweight region of the telescope, at a distance of the order of 12 m from the PM's.

II.2.3.2.2 Measurement of charge

We want a correct measure of the charge from 1 γe up to almost 1000 γe. In the following table we present a few useful numbers.

G PM	2×10^5	10^6	
I (μA) *	0.6	3	for 0.2 γe / 10 ns
Q (fC) 1 γe	32	160	
A (mV) 1 γe	0.8	4	for a signal width of 2 ns

* the limit recommended by the manufacturer is 30 μA.

In accordance with the circuit diagram we must divide the signal at the output of the PM's in two to go to the trigger line and the measurement line. The numbers appearing in the last two lines will be thus be divided by two for the measurement of charges.

The estimations which follow are done using the hypothesis of a PM gain of 10^6

Carte trigger T1

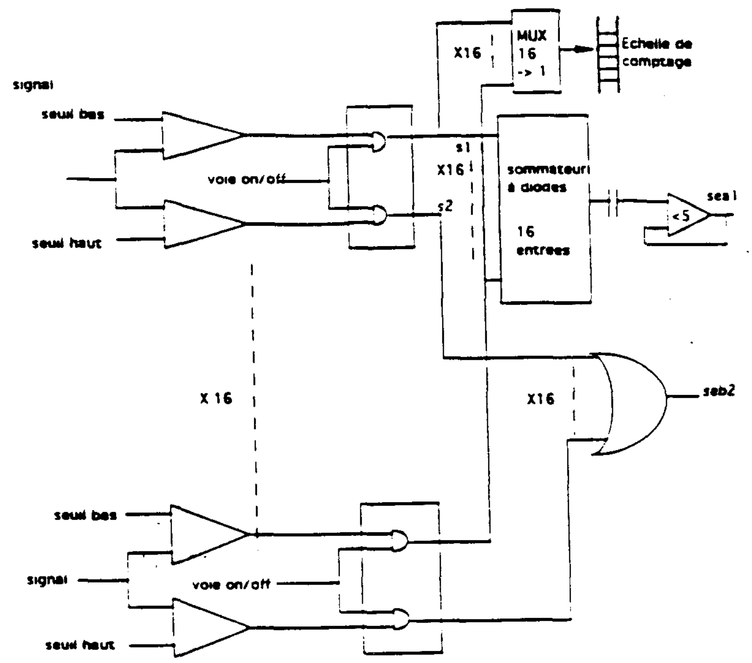

CARTE TRIGGER T2

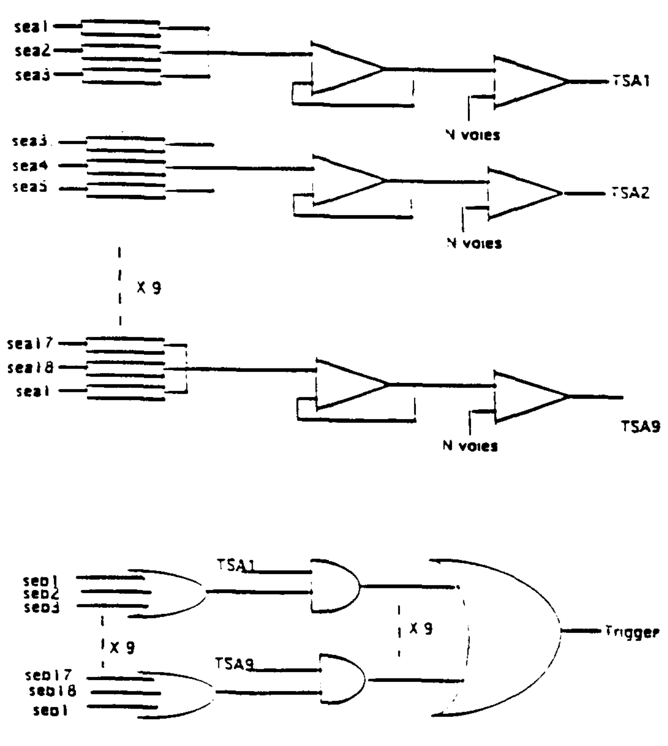

Fig.11 Diagram of the trigger logic

a) measurement of weak signals

We want to obtain a correct measurement of the charge corresponding to one γe. From the tests, the PM's give $\sigma_1/Q_1 = 0.4$ for the γe signal.

By choosing the one γe peak near 6 channels we obtain a sigma of 2.4 channels. These values must permit us to position the peak correctly and so to monitor the gain of each PM. For these weak signals, the intrinsic noise of the fast gate must stay far below 80 fC.

If we assume an ADC of 50 fC steps per channel, we see the necessity of amplification to obtain the single γe peak at 6 channels ($6 \times 50 = 300$ fC).

This amplification will be situated behind the analogue fast gate to avoid saturation in the case of strong signals. Thus, it does not require a very large bandwidth, and a relatively low gain is sufficient (≈ 4).

b) Measurement of strong signals

The fast analogue gate saturates at around 2 Volts; this limitation must not constrain our measurements.

The signal corresponding to one γe, after dividing by two, is 2 mV; the fast analogue gate saturates towards 1000 γe which is the maximal value that we have set ourselves. Any amplification of the signal before this gate would prevent us from obtaining this dynamic range

We will have, however, a loss of charge for those signals which spread over more than 10 ns.

Note that the single photo-electron level is found at 6 channels, fixing the capacity of the ADC:

11 bits 2000 channels gives 330 γe

15 bits 32000 channels gives 5300 γe.

A 15-bit ADC, of the Fastbus type, covers most of the useful dynamic range. However, if we use an 11-bit ADC, we must study the operation of a logarithmic amplifier.

STUDIES IN PROGRESS

The number of measurement lines obliges us to multiplex the lines before the ADC, which implies placing the signals into memory.

Several possibilities are under study:

- Use of Fastbus 1885 F ADC
  - Little electronic development
  - Awkward enough operation
  - Two different buses – Fastbus and VME
- Analogue memory developed by a team at CERN (P. Jarron)
  - Electronic development
  - Current limitation to 11 bits
  - The card studied includes the multiplexer, the ADC and DSP.
  - We use only partially the circuit potentialities because the analogue gate's upper limit is often reached by the trigger.

II.3 Operation of the imaging device

Towards a detailed exploitation strategy
Monitoring of pixels in real-time
Measurement of stars
Registration of an astronomical clock
Associated use of sampling and the imaging device

II.3.1 TOWARDS A DETAILED EXPLOITATION STRATEGY

The CAT imager constitutes a second-generation instrument, whose conception rests on an already well established expertise. The performance can be anticipated with some certainty, which will be the aim of the following chapter.

For the same reason, it is possible to establish in advance protocols of exploitation, defining the ways which we shall proceed at the site, in the same spirit which prevails for certain experiments on large machines. On this detailed preparation will depend, in part, the rapid acquisition of results from astronomical observations well as a good strategy for a large international project.

The protocols of exploitation will be detailed following the current work of evaluation. These programmes of simulations must be integrated with all available technical information as the tests and construction proceed.

The proper operation of these protocols presupposes that the on-line control devices are formulated in consequence; the general conception of these programs must be defined without delay.

From the point of view of the equipment, it is more important still to foresee concretely the critical performances because, in this domain, the choices will quickly become irreversible. From this perspective, we will outline below a few considerations in respect of the exploitation of CAT.

II.3.2 MONITORING OF PIXELS IN REAL-TIME

In this experimental high-definition imaging device, the possibilities of on-line monitoring become very important. The expected precision — on the noise and on the number of photons in the shower image, on the pointing of the telescope, etc. ... — presupposes the existence of good calibration and monitoring tools.

If the use of individual PM's is decided — instead of a smaller number of multi-anode PM's — their monitoring must at least be ensured, the more so since even a small variation of the gain implies a large shift in the count rate and since the gain varies rapidly with the voltage.

The good performance of the chosen PM's for the observation of single γe's (Fig. 7), will allow their gains to be calibrated absolutely before their installation. This calibration must also be achievable on-site.

During observations, the stability of the PM lines will be monitored using counters — below the comparators, thus typically above 4 γe — and by reading the charges in all pixels, including those which are far away from the shower, during the triggering events.

It will without doubt be useful to implement, at a higher rate and out of the triggering of events, readings of the ensemble of the camera; eventually the charge integration gate before coding by the ADC will be lengthened so as to optimise the information received about the noise. This tracking of the responses of all pixels should provide much information: on the stability of each line, on the possible increase of even weak noise (stars), even on individual gains. This information should be pre-treated by a rapid processor in the ADC crate.

II.3.3 MEASUREMENT OF STARS

Similar methods of tracking individual pixels in real-time should allow the observation of stars, if possible up to the 7th or 8th magnitude, that is to say up to light levels of two or three times the sky noise. As we have stated in chapter II.1 on the *observational data*, these data can be exploited to monitor the telescope pointing, the device luminosity, and the angular resolution of the optics. There again, the best procedure will have to be searched for and validated even before the ensemble is available.

II.3.4 REGISTRATION OF AN ASTRONOMICAL CLOCK

The search for possible modulation of cosmic gamma emitters imposes the use of an astronomical clock allowing analysis over long and discontinuous observation periods (mainly at night). Attention will have to be paid that the operation modes do not introduce parasitic frequencies which would be difficult to distinguish from a possible signal (this could come, for example, from the monitoring readings if they are taken at a fixed frequency).

II.3.5 ASSOCIATED USE OF SAMPLING AND THE IMAGING DEVICE

The trigger rate of sampling devices being of the order of a Hertz, it is seemingly easy to envisage the labelling of each event with a clock time which will would allow off-line association of the observations of the same shower by various devices on the site. It will be necessary to search for these correspondences even at the time of the observations. Tools will have to be developed towards this end, consisting in particular of the simultaneous on-line display, on consoles, of the various detectors.

For the imaging device, the response delay of the triggering logic being only $\approx$ 20 nsec, we have plenty of time to interrogate the sampling devices on their PM responses at the time corresponding to the same atmospheric event. The interrogation of the sampling devices may be useful even when it is an event which would not cause a the trigger. The procedures of synchronisation will have to be thought out in detail.

II.4 Principal performances expected of the imaging device

Conditions of simulation of the imaging device
Method of reconstruction and identification of showers
Performance concerning compact sources

We now present a first estimate of the expected performance of the imaging device from simulations, from the perspective of operation at the lowest possible energies and the capacity for observation of compact γ-sources. We limit ourselves here to the two following two principal aspects:

- the performance of the high definition imaging device
- the combined operation of the imaging device with the existing installations of ASGAT and THÉMISTOCLE.

II.4.1 CONDITIONS OF SIMULATION OF THE IMAGING DEVICE

The showers produced in the atmosphere by γ's or protons in the range 0.1 TeV to 5 TeV have been simulated with the UNICAS software (Ref. 13), already used by the Whipple Observatory group. We limit ourselves here to observation directions close to the zenith. The reflector, with 16 m^2 useful surface area, is placed in the centre of the field of mirrors of THÉMISTOCLE. We have considered the optimal solution for the camera (Fig. 8), the angular distance between the centres of two adjacent pixels is about 2 mrad. The photons are focused towards the sensitive zones of the photo-cathodes by the conic reflectors, reducing the effect of the dead-space. The global efficiency of production of a photo-electron (including the mirror reflectivity, the efficiency of the light collector, and the quantum efficiency of the PM) is taken to be equal to 20%. The PM response for n photo-electrons is Gaussian with a deviation equal to $0.4\sqrt{n}$, generally negligible compared with fluctuations in the number of photons in a shower of given energy. The 9 innermost rings of the tubes participate in the majority triggering logic. In the triggering strategy described above, the threshold of the comparator associated with a PM is fixed so as to require an average of 4 γe at least. The signals of the different comparators are then summed; the threshold of the associated discriminator is fixed so as to have at least 4 pixels satisfying the previous condition. The output signals of the PM's have been simulated, as have the responses of the comparators in the case where the photons come from sky noise as well as in the case where they have been produced by an atmospheric shower; in this last case, we take into account the anisochronism due to the optics of the reflector. We thus verify that the previous thresholds are sufficient to bring down the trigger rate due to sky noise to well below a Hertz.

II.4.2 METHOD OF RECONSTRUCTION AND IDENTIFICATION OF SHOWERS

The discovery of a compact source necessitates good discrimination between photons and hadrons. It is known that the change from 37 to 109 PM in the Whipple Observatory camera has brought decisive progress. To evaluate the performances of a camera with 546 PM, we have re-done from the beginning the analysis done for that experiment, including also a few refinements made possible by the higher resolution. This method does not use, however, all the available information and the criteria for separation of the signal and the background noise have not been optimised.

To maximally reduce the influence of the sky noise (0.1 to 0.2 γe / 10 ns), only pixels with more than 2 γe are taken into account in the analysis (this supposes that the reading does not extend over more than 20 ns). The photo-electrons created by the γ shower are hypothesised to be distributed according to a two-dimensional Gaussian law about their centre of mass B and the two principal directions and corresponding standard deviations (σ_L and σ_T ($\sigma_L > \sigma_T$)) can be determined (by maximum likelihood). These latter are expressed in mrad (as are all distances in the focal plane). This reconstruction is possible only if the determinant of the quadratic form associated with the Gaussian is positive, which assumes that the points are sufficiently grouped. Showers whose centre of mass is further than 19 mrad from the centre of the field of view O are also rejected; in this case, in fact, too great a number of the photons fall outside the field of the camera. The showers satisfying the previous conditions (Fig. 12) are characterised by :

- the distance d_B from the centre of mass B to the centre of the field of view O;
- the direction of the principal axis;
- the two standard deviations, longitudinal σ_L and transverse σ_T.

Table 2 gives average values for σ_L and σ_T for photon showers of energies between 0.3 and 4 TeV coming from the supposed source. Note that the fine grain allows σ_T values to be obtained which are greatly below to those from the data of the Whipple Observatory telescope (2.6 mrad).

A correlation between d_B and σ_T is also seen: the transverse standard deviation is larger for showers close to the centre of the field of view. This effect is particularly marked at energies

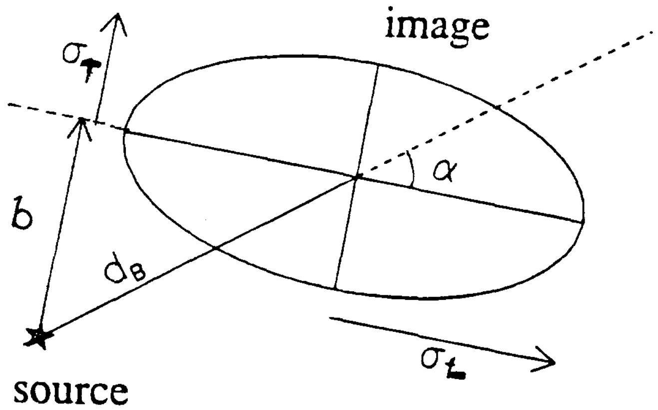

Fig.12 Definition of the image parameters

above a TeV (Fig. 13).

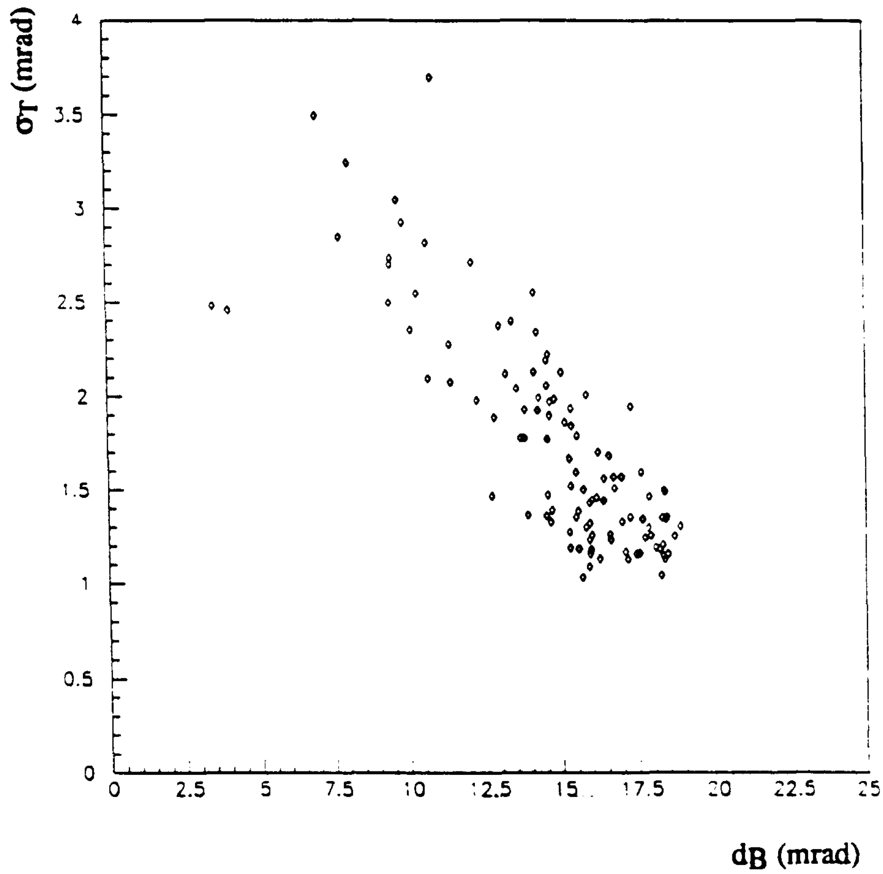

Fig.13 Correlation $\{\sigma_T, d_B\}$ for 4 TeV gammas parallel to the axis

The next step consists of verifying that the reconstructed shower points towards the supposed source at the centre of the field. The angular resolution is characterised by the angular impact parameter b defined in figure 12; for photon showers of fixed energies coming from the supposed source, the standard deviation of b is given in table 2. It is always less than 3 mrad. The pointing criterion decided upon for this analysis uses the angle α between the principal axis of the shower and the straight line OB, whose typical values are also shown in table 2. As these vary with the incident γ energy, the tolerance on α has been fixed as a function of the γe number; here it is about 9° at 4 TeV and 25° at 0.3 TeV. This cut rejects only 10% of the γ's. Whereas b represents a transverse angular deviation, no use is made of the direct information on the angular distance of B to the source along the principal axis. However, the correlation between d_B and σ_T provides indirect information. This shape-distance correlation is exploited in the next phase of the analysis.

Table 2 shows the correlation between the shower shape (defined by σ_L and σ_T) and the energy of the incident photon originating from the supposed source. For a number of γe and a given distance d_B, a "standard shape" can be defined (that is to say an average σ_L and σ_T). The deviation between the observed structure and the standard shape is characterised by a parameter H chosen such that its distribution is, for a γ-shower, independent of the energy; in our analysis it is a decreasing exponential of average value 1.3; for a shower created by a proton in contrast, H can take much bigger values (a few tens). To have effective rejection of the hadronic background, this parameter H is required to be less than 1. This test includes information on the correlation between the shower shape and the position of the source along the axis. Figure 14 shows the event distributions in the (H, sin α) plane for the γ-showers and the proton-showers respectively.

Table 2

E_γ (TeV)	σ_L (mrad)	$\Delta\sigma_L$ (mrad)	σ_T (mrad)	$\Delta\sigma_T$ (mrad)	$\Delta\alpha$ (mrad)	Δb (mrad)
0.1	2.7	1.0	0.76	0.34	250	3.2
0.3	2.9	1.0	0.76	0.34	140	2.1
0.5	3.3	0.96	0.89	0.40	120	1.9
1	3.9	0.72	1.1	0.45	79	1.2
4	4.7	0.63	1.7	0.57	57	0.52

Protons of energy below 200 GeV only contribute to the background by the presence of muons falling close to the detector; the latter produce images in the shape of rings or arcs which are easy enough to identify when they cover a sufficient number of pixels. A simple criterion based on the average value and the standard deviation of the number of γe per pixel allows us to eliminate most of them. Also, the very short arcs are efficiently rejected by the criteria of shape and orientation. The total factor of rejection of muons is of the order of 100.

In the following, we designate the steps of the analysis described above by the following symbols:

D : criteria of triggering;
P : " " orientation;
F : " " shape (parameter H and cut for muon rejection);
T : aggregate of criteria P and F.

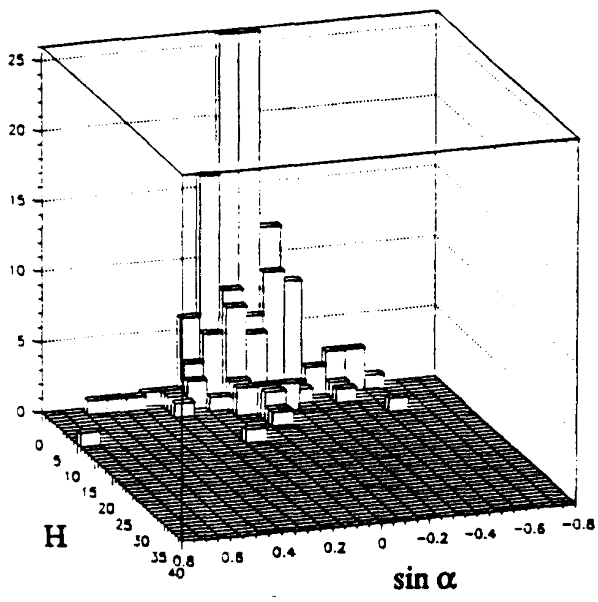

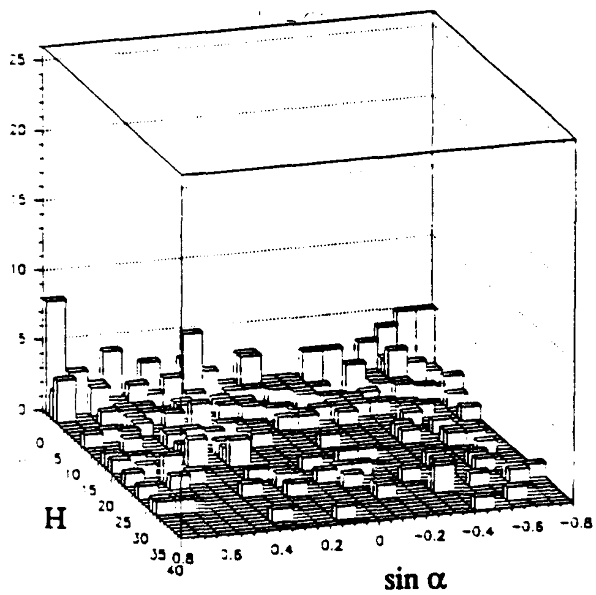

Fig.14 Distributions of events according to the hadronicity (H) and pointing (sin α) parameters respectively, for 300 GeV gammas (above) and protons (below).

II.4.3 PERFORMANCE FOR COMPACT SOURCES

The previous analysis is applied:

– on one hand to γ-showers originating from the supposed source.

– on the other hand to proton showers in a cone of semi-angle 40 mrad around the pointing direction, where the energies are distributed according to the energy spectrum of cosmic rays between 0.2 and 5 TeV.

The impact point on the ground of the shower axis (or shower foot) is assumed to be distributed uniformly in a radius of 200 m around the imaging device. For the photons emitted from the source, the acceptance of the apparatus is defined by:

$$A_\gamma = \int \varepsilon(r) 2\pi r\, dr$$

where r is the distance from the foot of the shower to the mirror and ε(r) is the probability to satisfy the trigger criterion (table 3).

Table 3

Acceptances for γ's, in 10^8 cm^2

E_γ (TeV)	0.2	0.3	0.5	1	4
(Triggers)	3.46	6.07	7.76	9.03	11.1

The acceptance is zero a little below 100 GeV, but increases very rapidly between 100 and 300 GeV (Fig. 15a). Figure 15b shows the number of events per second per TeV for the Crab Nebula at the given trigger level. The integral flux of γ's with energy above E (TeV) is 2×10^{-11} $E^{-2.4}$ cm^{-2} s^{-1}. The maximum of the curve (for the nominal trigger) is about 200 GeV (against almost 400 GeV at the Whipple Observatory with a 75 m^2 mirror). The efficiency of selection according to the combined criteria T depends little on the energy and remains of the order of 40%. It is also interesting to consider a source whose spectral index in the threshold region is high. The very distant quasar 3C279 emits a signal which is highly attenuated by the intergalactic infra-red light for energies of more than a few hundred GeV and has not been observed in the TeV region although it is the most luminous γ-source in the EGRET catalogue. The "low" estimate of the calculated flux by Stecker, De Jager and Salamon (Ref. 10) (solid curve in Fig. 16a) is quite detectable with the CAT imaging device (Fig. 16b), the rate of events after cuts being comparable that of the Crab Nebula, but with energies concentrated below 300 GeV. Table 4 gives the number of events satisfying the analysis criteria per hour of operation for the Crab Nebula and 3C279 respectively.

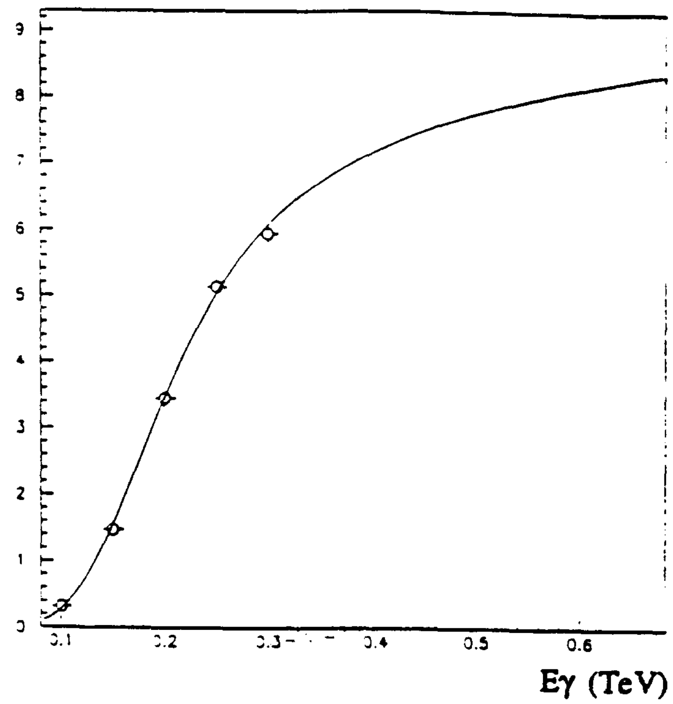

Fig.15-a Acceptance for gammas (by 10000 m²)

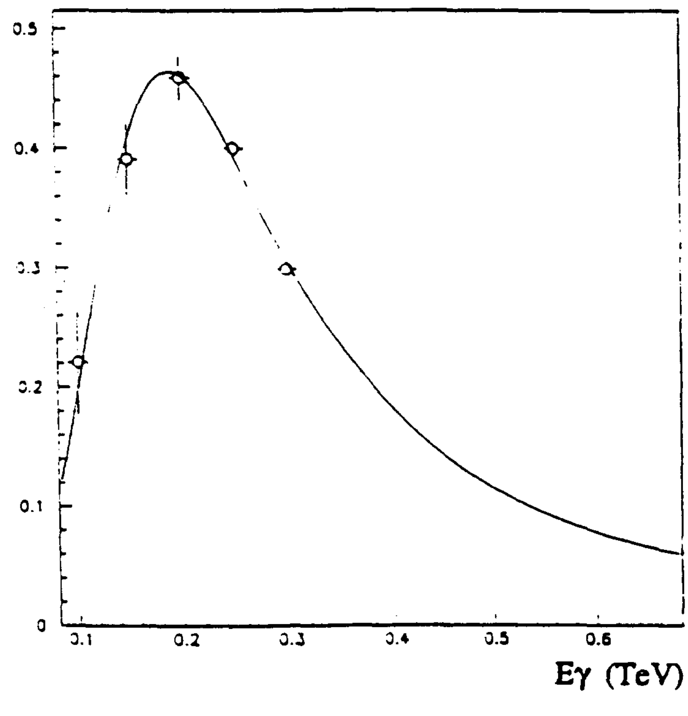

Fig.15-b Expected number of gammas from the Crab (per second per TeV)

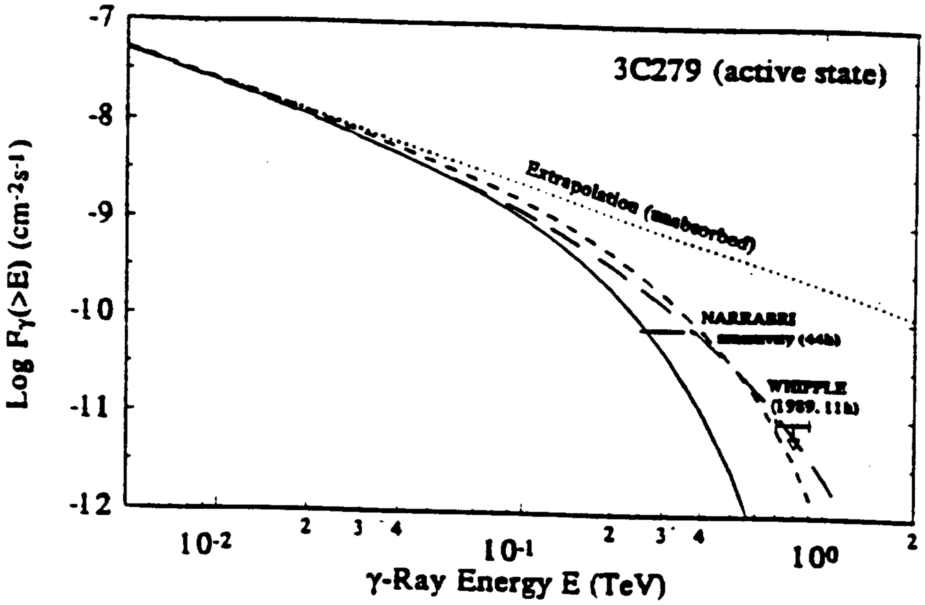

Fig.16-a Spectrum of AGN 3C279 with the effects of absorption by infra-red light (according to Ref. 10)

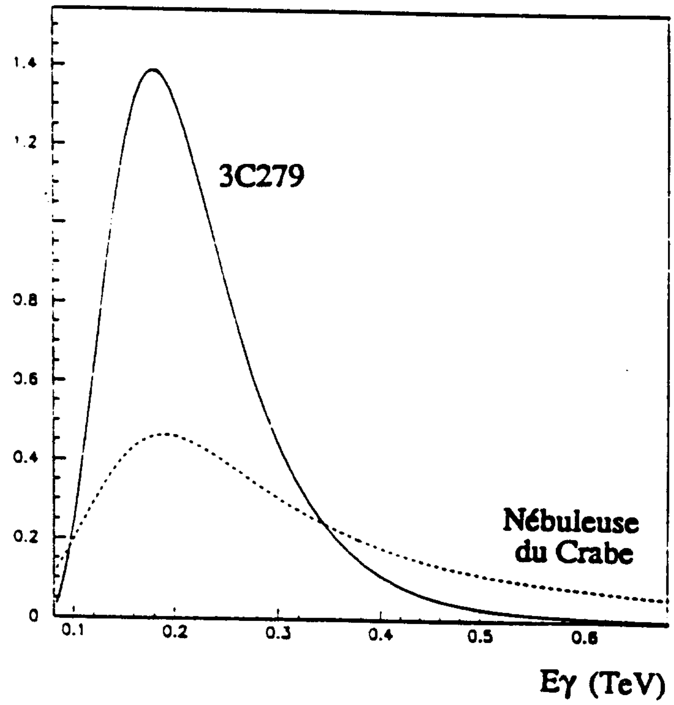

Fig.16-b Expected number of gammas from the Crab and AGN 3C279 (per second per TeV)

Table 4

Number of γ events per hour (signal S)

(after all analysis cuts for the Crab Nebula and the quasar 3C279)

	Crab	3C279
E > 150 GeV	218	315
E > 200 GeV	178	195
E > 300 GeV	113	49
E > 500 GeV	54	3
E > 1 TeV	18	—

For protons the acceptance is defined according to:

$$A_p = \iint \varepsilon(r,\theta)\, 2\pi r\, dr\, 2\pi\theta\, d\theta$$

where r and ε have the same meanings as above and where θ represents the angular distance between the centre of the field of view and the arrival direction of protons in the atmosphere. The values of A_p at different steps of the analysis are given in table 5.

Table 5

Acceptance for protons in 10^4 cm^2 sr.

(Proton energies between 0.2 and 5 TeV according to the integral spectrum $E^{-1.67}$)

D (Trigger)	19.3
P (Orientation)	1.77
F (Shape)	1.27

The rejection factor due to the orientation criterion remains at about 10 and varies little with the shower energy. In contrast, the rejection factor due to shape increases approximately as the square root of the energy: it is of the order of 15 at 200 GeV and 25 at 500 GeV. The combined rejection can only be estimated precisely with very high statistics from simulations; around 200 GeV, in the most unfavourable conditions, the total factor of rejection is about 100. Note that at low energies, the trigger conditions for a γ-shower are fulfilled only for distances to the shower foot less than 150 m; the telescope is, however, sensitive to showers of protons at a distance of about 200 m because the secondaries of the hadronic cascade make larger angles with the average direction of the shower. The trigger rate due to hadrons is close to 40 Hz but may be reduced by a factor of almost 2 by the sector division of the PM's of the camera (not yet included in the simulations). After analysis a background of B = 1600 events per hour is obtained. The significance of the signal from the Crab Nebula is:

$$\frac{s}{\sqrt{B}} = \frac{218}{40}\sqrt{t_{hour}} \approx 6\sqrt{t_{hour}}$$

or, more rigorously:

$$\frac{"ON"-"OFF"}{\sqrt{"ON"+"OFF"}} \approx 4\sqrt{t_{hour}}\,.$$

In conclusion, an imaging device of 16 m², a surface almost four times smaller than the Whipple Observatory's will:

- have a nominal threshold of 200 GeV (against 400 GeV of the Whipple Observatory), which represents a gain of a factor of 2 or 3 in the rate of events;
- keep a comparable sensitivity (5σ in one hour for the Crab Nebula);
- be likely to discover active galactic nuclei whose γ radiation is highly attenuated by the intergalactic infra-red radiation, like 3C279.

III. Development of the sampling devices (ASGAT and THÉMISTOCLE) and their associated exploitation with the imaging device

III.1 Improvements in sampling devices

III.1.1 THÉMISTOCLE

With the intention to simultaneously use imaging techniques and time measurements, it is critical to improve immediately the ensemble of THÉMISTOCLE and undertake a certain amount of research and development with a view to participating in a future far-reaching international collaboration.

III.1.1.1 Improvements

The current photo-multipliers are reused from the DM2 experiment. Their antiquity give them reduced performances with respect to currently produced photo-multipliers. We propose their replacement by XP2020 Q photo-multipliers, which may or may not be used with UV filters.

III.1.1.2 Research and development for the future

Among the information gained from the THÉMISTOCLE experiment, two points are important:

- Sampling by 18 telescopes limits the possibilities. It would be desirable to increase the number.
- the transfer of information by cables to a central location before making the decision limits the performance of the detector and is not adapted to a large-scale experiment.

These two points will be taken into consideration in the proposal of improvements.

1) Improvement in time measurement

The complete treatment of the signal must be made closer to the photo-multiplier so as to use the characteristics of the rapidity of the pulse to best advantage. The analysis of the signal near the head of each heliostat necessitates the storage of data when waiting for the trigger. This situation implies the development of an integrated *multi-hits* TDC whose characteristics must satisfy the conditions of the experiment (large dynamic range, not ≤ 100 ps)

2) Improvements in energy measurement

The current measure of the energy, taken after 300 m of cable, necessitates the integration of the signal over 200 ns. Many background sky-photons are accumulated in this gate width so the precision of the measurement is limited. We propose to move this measurement to each heliostat. This will require a study of analogue memory, followed by an ADC.

To increase the dynamic range we are studying the possibility of using the intermediary signals of the dynodes.

On the other hand, we wish to study a mirror configuration (size and tracking mechanics) towards the prospect of a future experiment and with the goal of improving the Cherenkov light to background sky ratio. For this we will deposit a specific demand of investment at the end of 1994.

III.1.2 ASGAT

The improvements to ASGAT will consist mainly of the individual analysis of the 49 PM's in the experiment. This new device will allow greater flexibility in the trigger logic as well as better reliability in the control and operation of the experiment. A significant decrease of the threshold energy of the telescope is also expected, and thus better sensitivity for detection of gamma sources. The combined operation with the CAT imaging device will also be greatly facilitated.

III.2 Interconnection of sampling devices and the imaging device

The guidance of the CAT ensemble is carried out from a workstation connected to each of the three detectors; i.e., the imaging device, ASGAT, and THÉMISTOCLE. This workstation must ensure the following functions:

- the acquisition of data from the imaging device itself
- the control and on-line surveillance of the three detectors
- the collection of the data from ASGAT and THÉMISTOCLE
- the synchronisation, the formatting, and the storage of all data
- the execution of programs of monitoring, control, tracking, ... on each of the detectors separately or as a whole

An *Ethernet* fibre-optic network will be used to connect between the three detectors and the site of the central workstation. A schematic representation is shown in Fig. 17.

The workstation will operate under UNIX, fairly powerful (e.g.: DEC 5000-240, HP 715/33 ...) with a fairly large disk, backup (DAT), and a CD-ROM reader. Moreover, we require a maintenance contract with intervention in 48 h maximum.

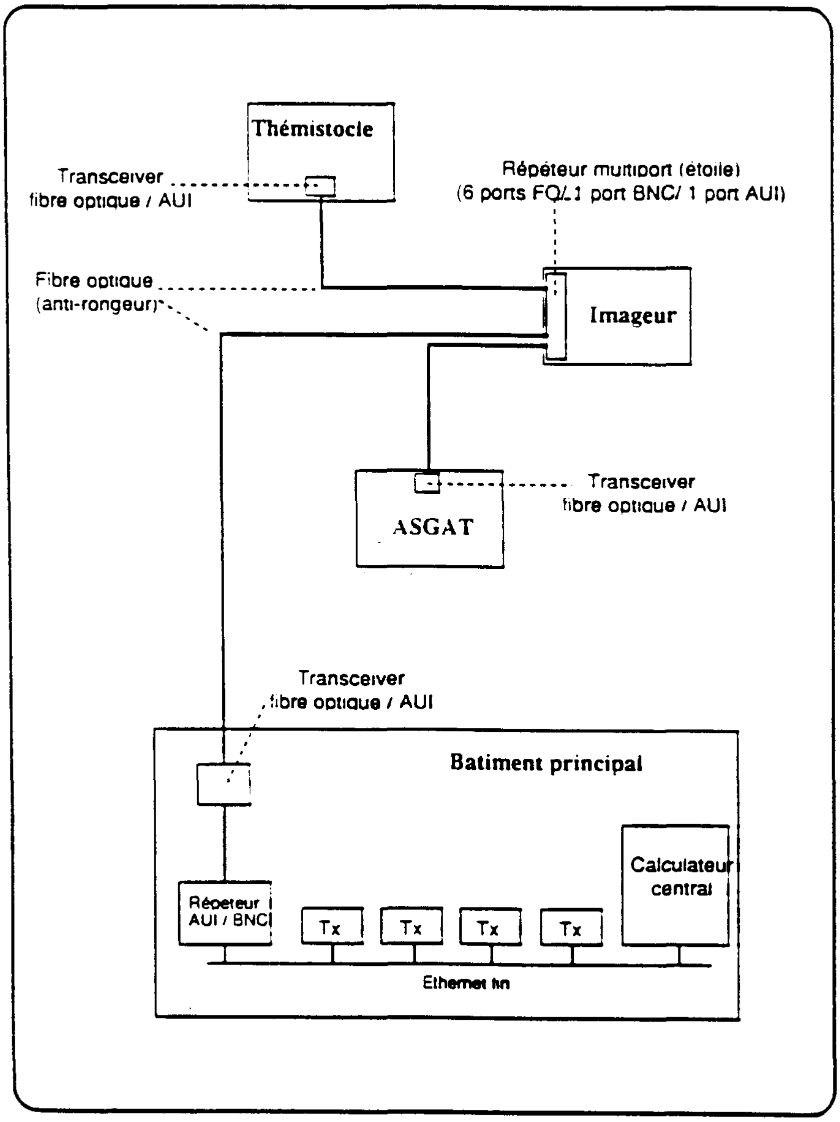

Fig.17 Network architecture

III.3 Performance expected from the association of imaging / sampling devices

The two existing detectors, ASGAT and THÉMISTOCLE, work in different energy domains. Each of them can, however, take advantage of the information of the imaging device on the position of the shower foot. We show first how this can be reconstructed from the shower image, then we estimate the advantages which result for the sampling detectors.

III.3.1 Reconstruction of the shower impact point by Cherenkov imaging

For a γ-ray of given energy emitted from the observed source, there is a strong correlation between the distance D from the imaging device to the shower foot and the angular distance d_B = OB defined above (Fig. 18).

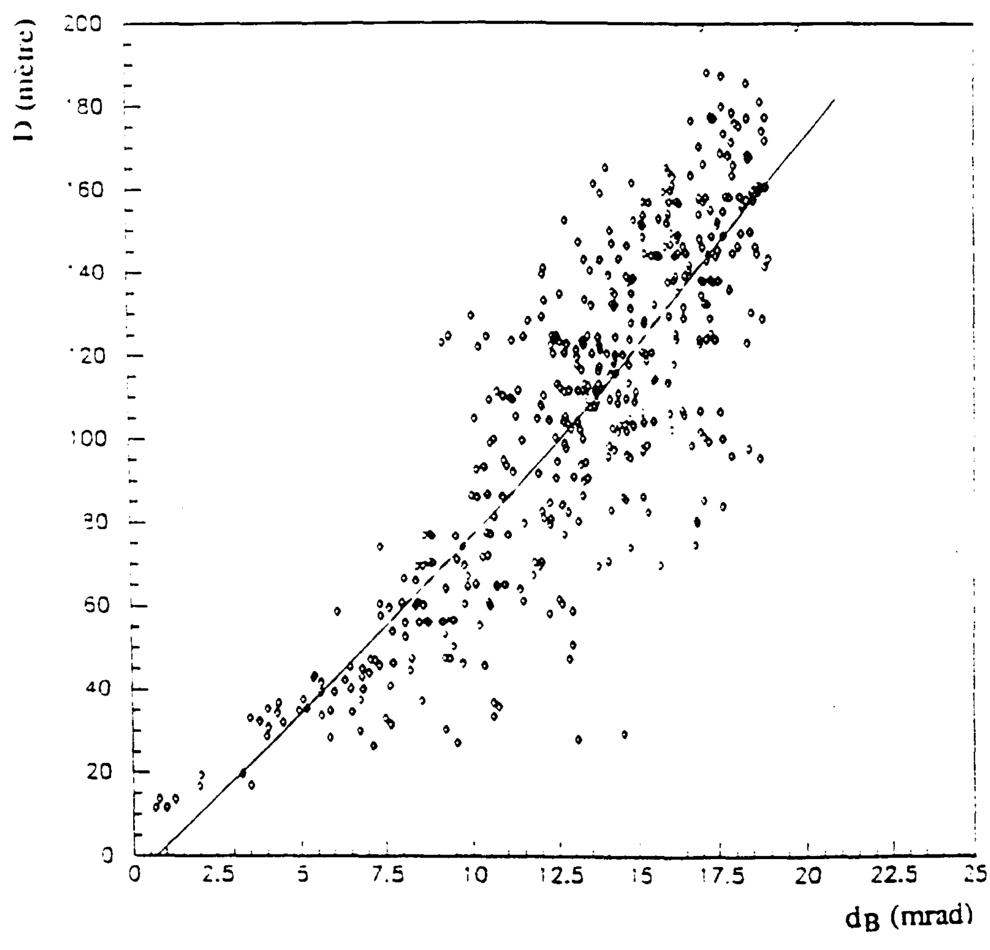

Fig.18 Correlation between the distance to the shower foot and d_B (the angular distance between the barycentre and the sighted point)

The functional relation linking the average of d_B to D depends greatly on the γ's energy. An estimator function $\Delta(d_B, N_{\gamma e})$ of the angular distance d_B and the number of photo-electrons detected can be defined whose average value is $D^{\cdot}$ and whose distribution is approximately Gaussian (fig. 19). The standard deviation of the distribution obtained roughly follows the law

$$\sigma(\Delta\text{-}D) = 1.63 \text{ m} - 4.4 \text{ m} \log_{10}(E/\text{TeV}) \qquad (1)$$

which gives 18 m at 0.3 TeV and 14 m at 4 TeV. This positions the shower foot in the radial direction with respect to the imaging device. In the transverse direction, the error is D.Δα where Δα is the standard deviation of the angle of deviation α (Table 2). For D = 100 m the transverse error is 14 m at 300 GeV and 6 m at 4 TeV.

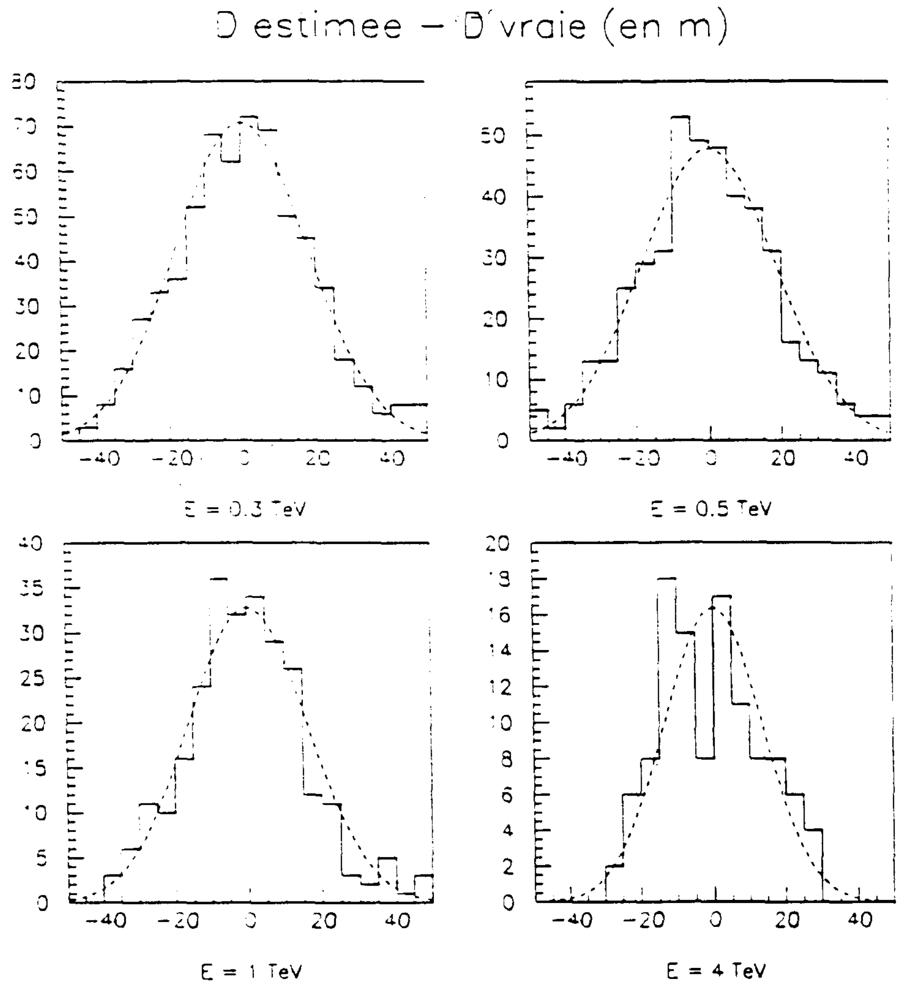

Fig.19 Determination of the shower foot by the imaging device: resolution as a function of energy

III.3.2 USE BY ASGAT AND THÉMISTOCLE OF THE RECONSTRUCTION OF THE SHOWER FOOT FROM IMAGING

From its relatively small lever arm, ASGAT reconstructs a plane wave-front and cannot determine the impact point from its own data. This results in a parallax error of 0.7° (12 mrad) in the source direction (Ref. 5). By using data from the imaging device, the angular resolution will be of the order of the ratio between the error on the position of the shower foot (~ 18 m) and the distance to the maximum development of the cascade (~ 6000 m); i.e., 3 mrad. This gain of a factor of four in angular resolution (which has repercussions as the square of the background of unrejected hadrons) has an effect on the significance of the signal.

Using a more extended mirror field and working at higher energies where the wave-front has a more conical form, THÉMISTOCLE determines the shower foot from the data from 12 stations. This condition allows sufficient constraints in the procedure of reconstruction of the cone which uses 12 data items (the arrival times of the Cherenkov signal at the different stations) for 6 unknowns (the 2 co-ordinates of the impact point; the arrival time of the wave-front at this point; the 2 angles defining the direction of the cone axis; the opening angle of the cone). The uncertainty Δr on the position of the shower foot is then 15 m on average and fixes the angular resolution approximately according to $\Delta\alpha$ (mrad) = 0.17 Δr (m); i.e. 2.6 mrad. However, the requirement that 12 stations be hit is one of the factors which limits the operation of THÉMISTOCLE at energies above 3 TeV (the other factor being the threshold of the PM discriminator set at 9 γe; i.e., 4σ above the sky noise). The independent determination of the foot of the shower by the imaging device reduces the number of unknowns to 4 and gives the same number of constraints if 10 stations are required to be hit. In these conditions, by decreasing the threshold of the each PM's discriminator to 6 γe*, the threshold can be lowered to 1.5 TeV by determining the position of the shower foot from the imaging device. Formula (1) then gives an uncertainty of 15.5 m; the angular resolution, which is proportional to it, is then 2.6 mrad (as for 3 TeV shower observed under current conditions). The gain in statistics of events emitted from the Crab Nebula is then $2^{1.4} = 2.6$.

The imaging device also brings with it its intrinsic criteria of hadronic rejection, that is to say largely independent of angular criteria already available from the sampling detectors; at energies above a TeV, this rejection factor due to the shape of the image alone is of the order of 50. Even if it is related only partially to the information already used by THÉMISTOCLE, it must yield a large reduction in the hadronic background.

* With a PM threshold of 6 γe, the individual count rate rises to 20 kHz; the probability that one of the ten stations hit would be polluted by the random "stop" of a TDC is only 10%. The trigger rate with 10 stations is then 0.6 Hz. The uncertainty in shower energy is then $\Delta E/E$ = 28% for a γ-shower (as against 20% with the current conditions of operation at 3 TeV).

III.3.3 CONTRIBUTION OF SAMPLING DETECTORS TO THE IMAGING DEVICE

Reciprocally, the detectors of ASGAT and THÉMISTOCLE usefully complement the imaging device.

So, to reject the gamma candidates which are in fact muon images or the effects of the interaction of cosmic rays with the camera — darts — the ASGAT telescopes must be interrogated. It has been shown that for 200 (150) GeV gammas, in 95% (80%) of the cases, at least one of the ASGAT telescopes gives a signal above threshold.

Moreover, THÉMISTOCLE has an extended mirror field which exhibits advantages regarding the measurement of energy: in this case, the photons collected by the ensemble of mirrors are truly representative of the development of the entire shower and do not favour any altitude of emission if the shower foot falls in the area defined by the outermost stations. However, a single imaging station always preferentially samples an altitude range depending on the distance to the shower foot. Also, the energy measurement by the imaging device depends not only on the single datum of the number of photo-electrons, but also on d_B; i.e., position of the shower foot. Comparison with the THÉMISTOCLE data will be essential to verify or correct the energy estimations obtained from the simulations.

IV. Division of tasks/ calendar/ costs

IV.1 Organisation of the site

We anticipate here the problems of staff and organisation linked to the installation and operation on the site, as well as the infrastructural problems related to the installation of the imaging device.

IV.1.1 PERSONNEL

With regard to the installation of the imaging device and in the perspective of the multiple use of the site, it is necessary that the co-ordination of the whole be overseen by a physicist in charge of the site.

From the beginning of September '93 a technician's post (T3 level) must be provided for the CAT experiment. This technician would have to spend some time in the related laboratories as training. In the first stage, the technician will be linked to one of these laboratories.

Before the installation on site of the imaging device, planned for mid-95, an engineering post (IE level) earmarked for the site would be very useful. This engineer, helped by the technician, would have to look after the tracking of the operation of all the apparatus of the experiment. The engineer would also participate in its improvement in collaboration with the whole staff. The engineer and technician must live near the site, with possible displacements to the different laboratories of the IN2P3, DAPNIA, or the University of Perpignan.

These people will be under the supervision of the above-mentioned physicist. Later, dependent on the future of the site and the development of the University of Perpignan group, this group could assume the technical responsibility for whole.

IV.1.2 INFRASTRUCTURE

– *Shelter for storage and the mount*

It is critical to have a building to protect the vehicles necessary for the assembly and adjustment of the heliostats or to store the imaging device elements and there to perform certain assemblies.

The provision of a part of the factory ($\approx$ 100 m^2) would satisfy these needs perfectly. Alternatively, the construction of an equivalent area would be necessary the cost of which can be estimated at 300 kF.

– *Expansion of the telephone and electrical networks*

The imaging device shelter must have an electrical supply (with circuit breaker and installation) and contain a telephone link. We must consider changing the switchboard, with an increase in the number of lines. It is also useful to anticipate a telephone link close to the laser near the base of the tower and in the new offices.

– *Information link with CC IN2P3*

The current link under *Transpac* is being changed to *Numeris*. The expansion of the network in view of the action plan is under the responsibility of CC-IN2P3.

– *Vehicles*

The purchase of a second express-type vehicle is to be considered. In the near future the replacement of the first vehicle, currently used on the site, is anticipated.

– *Ongoing maintenance by the owner of the site.*

We ask that the site be regularly maintained to allow its trouble-free utilisation (road network, drainage, tower, offices, ...)

– *Security*

In a manner still to be defined, the security of installations will have to be ensured.

IV.1.3 OPERATING COSTS

Currently for THÉMISTOCLE the operating costs (EDF, telephone, cleaning, car maintenance, Odeillo shop ...) are of the order of 150 kF a year. For the operation of the site a sum of 350 kF would have to be foreseen from 1995 for the whole experiment (imaging device, THÉMISTOCLE, ASGAT).

IV.2 Allotment of tasks

Mechanics and Optics	
Conception and tracking of mechanical manufacture	X
Choice of mirrors and tracking of fabrication	id.
Device for verification of mirror alignment	id.
Installation of the telescope on site	id.
Camera	
Fabrication tracking and calibration of PM's	Dapnia
Conception and realisation of the camera box	id.
High voltage PM supply	X or Ir. ?
Electronics	
Fast trigger logic (study and realisation)	Paris 6-7
Measure of charges (ADC)	id.
Information	
Off-line simulations (physical and instrumental)	X (+ all)
Acquisition software for the imaging device	Paris 6-7 +X
Infrastructure: central computer and interconnections	Dapnia
Software for visualisation of experiments	CdF(+ all)
Telescope tracking	X
Administration on the site	? + Perpignan

IV.3 Costs

<u>Telescope</u>			
General Mechanics		700 kF	
Mirrors		700	
Upper sections and various		300	
Shelter and trolley		300	
	Sub total:		2000
<u>PM's and Camera</u>			
PM's (mixed version)		1800	
Mechanics and various		300	
High voltage supply		300	
	Sub total		2400
<u>Electronics</u>			
Fast logic		500	
Charge readers (ADC)		500	
Connections		400	
Various		100	
	Subtotal		1500
<u>Cost of whole project (incl. ASGAT and THÉMISTOCLE)</u>			
Computers and electronics		350	
Infrastructure*		400	
Development of THÉMISTOCLE		350	
	Subtotal		1100
Total..			7000 kF
plus 15% for unexpected events and various			1000
prototypes and developments			500
	General Total		**8500 kF**
	Operating costs		**350 kF / yr**

* Under this heading "infrastructure" we include one third for the working installations (electricity, phone), another third for the embanking and various and the final third for the expenses of partial renovation of vehicles. However, the sum of ≈ 300 kFr that would have to be spent in the case where the EDF factory would not be available for the storage of materials for maintenance is not included.

IV.3 Calendar

Mechanics and mirrors	
Quality control of mirrors	end 1993
Specifications of the mechanics (and prototypes)	id.
Signing of worksheets (mechanics and mirrors)	summer 1994
Arrangement on the site (flagstone, shelter, etc...)	mid 1994 – mid 1995
Mounting on the site	summer 1995
PM's and Camera	
Study of camera box	end 1993
Signing of worksheet on PM's	summer 1994
Realisation of box and PM calibration	1st semester 1995
Electronics	
Tests and technical choices	end 1993
Realisation of printed circuits	1994
Signing of worksheets	1994
Mounting and tests	1995

Table: Calendar of finances (in kF)

	1993	1994		1995		1996	Total
Telescope:							
mechanics		700					
mirror			1000				2000
shelter				300			
Camera:							
mechanics			200	100			
PM's			1800				2400
High voltages			100	200			
Electronics:							
ADC (Fastbus)	300			200			
triggering		200	300				1500
connections				400			
various					100		
Acquisition:							
VME	100						
Workstation			100				350
Fibre Networks	150						
THÉMISTOCLE:							
PM's	150						350
Electronics				200			
Infrastructure:			100	200	100		400
Prototypes:	500						500
Total	1200	900	3600	1600	200		7500

Table: Budget for pre-studies and prototypes (1993)

	June 1993	October 1993	Total
Electronics – Paris 6	70 (light source + modules)	100 (proto cards + scope)	170
Mirrors – X		130 (prototypes)	130
PM Tests – X	75 (Hamamatsu and DEP + various)		75
Prototype Camera	125 (20 PM)		125
Total	270	225	500

References

1. H.E. Haber, G.L. Kane, Phys rep 117 (1985) 75.
2. G.B. Gelmini, Nucl. Phys B (Proc. Suppl.) 28 A (1992) 254.
3. F.A. Aharonian, P. Bhattacharjee, D.N. Schramm, Phys. rev. D 46 (1992) 4188.
4. T.C. Weekes et al., ApJ. 342 (1989) 379.
   G. Vacanti et al., ApJ. 377 (1991) 401.
5. P. Goret et al., A&A 270 (1993) 401.
6. P Baillon et al, Proc. XXVI ICHEP, Dallas 1992. To appear in Astro-Particle Physics.
7. F. Krennirich et al., Proc. XXIII ICRC, Calgary 1993.
8. S.Ogio et al., Proc. XXIII ICRC, Calgary 1993.
9. M. Punch et al., Nature 358 (1992) 477.
10. F.W. Stecker, O.C. De Jager, M.H. Salamon, ApJ. 390 (1992) L49.
11. M. Urban et al., Phys Lett. B 293 (1992) 149.
12. W. Stamm, K. Sauerland and N. Müller, N.I.M. A 328 (1993) 601.
13. M.P. Kertzmann, G. Sembroski, to appear in N.I.M.

Imprimerie de l'Ecole polytechnique - Palaiseau